FERROELECTRICITY IN THE TRANSITION METAL

CHALCOGENIDE, CU$_2$S, CHALCOCITE

A Thesis

by

MARK ZYGMUNT BIENIULIS

Submitted to the Graduate College of
Texas A&M University
in partial fulfillment of the requirements for the degree of

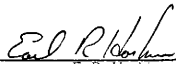MASTER OF SCIENCE

May 1985

Major Subject: Geophysics

FERROELECTRICITY IN THE TRANSITION METAL
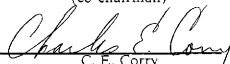
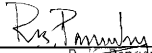CHALCOGENIDE, CU_2S, CHALCOCITE

A Thesis

by

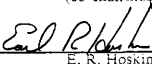MARK ZYGMUNT BIENIULIS

Approved as to style and content by:

_____
E. R. Hoskins
(co-chairman)

_____
C. E. Corry
(member)

_____
R. R. Pandey
(co-chairman)

_____
E. R. Hoskins
(Head of Department)

May 1985

ABSTRACT

Ferroelectricity in the Transition Metal

Chalcogenide, Cu_2S, Chalcocite (May 1985)

Mark Zygmunt Bieniulis, B.S., SUNY College at Brockport, N. Y.;

B.S., University of Arizona

Co-Chairmen of Advisory Committee: Dr. E. R. Hoskins
                                          Dr. R. K. Pandey

    The dielectric permittivity and conductivity of chalcocite were investigated as a function of temperature to determine if chalcocite is a ferroelectric mineral. Nonlinear behavior is observed, with anomalous changes in permittivity and conductivity at the order-disorder phase transition at 105° C.   Polarization reversal and dielectric nonlinearity as a function of applied electric field is demonstrated by dielectric hysteresis loop.   Such behavior is characteristic in known ferroelectric minerals and; hence, chalcocite is probably also ferroelectric.

ACKNOWLEDGEMENTS

I would like to thank my committee and all those people who helped in making this thesis a success. This research was inspired by Dr. Corry as result of his investigations into the natural electrical polarization phenomena associated with sulfide ore minerals. Dr. Hoskins provided the financial support and computer time to undertake this endeavor. Special thanks to Dr. Pandey for his insight and guidance with the experimental work. I am very grateful to the Solid State Materials Research Lab of the Electrical Engineering Department for the use of equipment and facilities without which this research could not have been done.

TABLE OF CONTENTS

Table of Contents (Continued)

LIST OF FIGURES

List of Figures (Continued)

LIST OF TABLES

CHAPTER I

INTRODUCTION

The objective of this thesis is to characterize the dielectric behavior of the mineral chalcocite, Cu_2S, as a function of temperature and applied electric field, in order to determine if its known phase transition at 105°C is ferroelectric in nature.

Ferroelectric crystals are characterized by a spontaneous electrical polarization which can be reversed by application of an electric field. It is well established that ferroelectric materials exhibit significant dielectric anomalies at their transition temperatures, known as Curie points, where the transition from an ordered polar phase to a disordered nonpolar phase takes place.

Chalcocite was chosen as a good candidate for ferroelectric behavior based on known structural, electrical and optical properties. A great deal of research has been done previously to characterize the phase transitions of cuprous sulfide. However, the literature is rather sketchy regarding the dielectric behavior of chalcocite at its transition temperature(s). My research has shown that there is definitely an anomaly in the dielectric permittivity and conductivity at the transition temperature, 105°C. Dielectric hysteresis is also observed, indicative of polarization reversal and; therefore, ferroelectricity has been established in the Cu_2S samples studied.

The investigation of the dielectric properties of Cu_2S is of considerable interest to the solid state industry because of the potential use of copper sulfide in

_____

This document follows the style of the journal *Geophysics*

solar cells and other semiconducting devices. Knowledge of the dielectric properties of minerals is also of fundamental importance in the application of electrical prospecting methods for copper and other metallic ores.

Sulfides constitute one of the few remaining groups of solids that are relatively unexplored and unexploited (Azaroff, 1975). Current research on the physical properties of sulfides has centered around semiconductors, photoconductivity and ferroelectricity (Pickart, 1970). Only a few sulfide minerals have presently been established as ferroelectric. None have yet been shown to be antiferroelectric (Lines and Glass, 1977).

My research has important implications for geophysical exploration for sulfide ore minerals. Sulfide mineralization is very common in nature and forms the ore minerals for most metals. Often, the concentrations of sulfide minerals can exceed 50% of the rock mass (Park and MacDiarmid, 1975).

The spontaneous polarization, or self-potential, method is often used in exploration for sulfides because they commonly show negative electrical anomalies with amplitudes which may exceed 1 volt. Sulfide mineralization is also known to produce an induced polarization effect, characterized by transient decay in the voltage across a body of mineralized rock when an applied current is abruptly discontinued. Various aspects of the spontaneous polarization (see Sato and Mooney, 1960, Corry, 1985) and induced polarization (Sumner, 1976) phenomena have been extensively investigated in the literature. However, the ferroelectric contribution of individual crystals or as semiconductor ceramics to the natural polarization phenomena observed in the field has not previously been considered, e.g. see Olhoeft, 1981. Parkhomenko (1971) investigated the piezoelectric and pyroelectric properties of rocks and minerals, and strongly suggested that further research on the ferroelectric properties of minerals be carried out. However,

work in this area has been very limited.

Corry (1984) has shown that over a 1 km stockwork porphyry sulfide deposit containing a diverse mixture of sulfides (FeS_2, $Fe_{1-x}S$, MoS_2, ZnS, PbS, Ag_2S, etc.), applied electric fields directionally polarize the entire rock mass even though the sulfides are known to be radially distributed.

The fact that a sulfide deposit can be directionally polarized has led to the question of whether the crystallographic phenomenon of ferroelectricity can be contributing to the observed field effects? An investigation of sulfide ore minerals by Corry (1984) has shown that many ore minerals do have structural, optical and electrically anomalous behavior which may be ferroelectric in origin. Pyrrhotite ($Fe_{1-x}S$), which does occur in the sulfide body tested by Corry and very commonly elsewhere, bismuthinite (Bi_2S_3) and stibnite (Sb_2S_3) are all established ferroelectric sulfide minerals (Lines and Glass, 1977). Furthermore, many sulfides are also isostructural with the known ferroelectrics.

CHAPTER II

DIELECTRIC PROPERTIES OF MINERALS

To appreciate the significance of ferroelectric behavior in minerals, and to be able to distinguish ferroelectrics from "ordinary" dielectric materials, it is important to understand the basic dielectric properties of minerals.

A dielectric material may be characterized by limited movement of charged particles or orientation of polar molecules when an external electric field is applied (Parkhomenko, 1967). A homogeneous dielectric medium inserted between two parallel metal plates will cause electric charges to accumulate on the plates. The increase in the amount of capacitance (C) relative to that of free space (C_0) is related by the relative electric permittivity of the material, ϵ_r.

$$C = \epsilon_r C_0 \tag{1}$$

Often referred to as the dielectric constant, ϵ_r represents the ratio of the electric permittivity of the dielectric to the electric permittivity of free space, ϵ_0 ($\epsilon_0 = 8.854 \times 10^{-12}$ F/m)

$$\epsilon_r = \epsilon/\epsilon_0 \tag{2}$$

If the dielectric is an anisotropic crystal, the permittivity and; hence, the dielectric constant may strongly depend upon the orientation relative to the crystallographic axes.

The increase in charge storage capacity is the result of polarization charges. By definition, the capacitance (C) of a dielectric is directly proportional to the total charge (Q), and inversely proportional to the potential difference (V) across the dielectric (Loeb, 1961).

$$C = Q/V \tag{3}$$

The appearance of polarization charges therefore increases the capacitance. Known as dielectric polarization, (**P**), this phenomenon results from the action of the electric field inducing a dipole moment.

P is proportional to the applied electric field intensity (**E**). In isotropic materials, **P** is a vector parallel to **E** such that the following linear relationship exists.

$$\mathbf{P} = \chi \epsilon_0 \mathbf{E} \tag{4}$$

The parameter χ is referred to as the dielectric susceptibility. In anisotropic materials the magnitude of **P** depends upon the direction of relative to the crystal axes. Therefore, the dielectric susceptibility may be considered in tensor form (Nye, 1979):

$$\mathbf{P}_i = \epsilon_0 \chi_{ij} \mathbf{E}_j \tag{5}$$

When an electric field passes through a polarizable medium, the resultant electric flux density (**D**) is directly proportional to the electric field intensity (**E**) and the electric permittivity (ϵ) of the medium.

$$\mathbf{D} = \epsilon \mathbf{E} \tag{6}$$

Since **D** arises from the total charge density and **E** arises from the real, or free charge density, for dielectrics the polarization (**P**) arising from the induced charge density must be included. Therefore:

$$\mathbf{D} = \epsilon_0 \mathbf{E} + \mathbf{P} \tag{7}$$

From equations (4), (6) and (7) we see that:

$$D = \epsilon_0 (1+\chi)E \qquad (8)$$

so $\epsilon_r = 1+\chi$ and the dielectric constant will always be ≥ 1.

As with the susceptibility (χ), the electric permittivity (ϵ) is a scalar for isotropic media, and a tensor for anisotropic media with the general form:

$$D_i = \epsilon_{ij} E_j \qquad (9)$$

In an applied electric field positive charges will be displaced from the negative charges in the direction of the field. This displacement can be represented by an electric dipole moment (p) with charge Q and charge separation d:

$$p = Qd \qquad (10)$$

The polarizability, a, is considered as the ratio of electric dipole moment (p) to the local electric field intensity (E_{loc}).

$$a = p/E_{loc} \qquad (11)$$

The polarization is then a measure of the induced dipole moment of N_i atoms, or ions per unit volume. The total polarization (**P**) can be written as:

$$P = \Sigma_i N_i p_i = E_{loc} \Sigma_i N_i a_i \qquad (12)$$

The total polarizability (a) can be expressed as a sum of four contributions:

$$a = a_e + a_i + a_d + a_s \qquad (13)$$

Electronic polarizability, a_e, results from the displacement of the generally symmetrical electron cloud relative to the nucleus of an atom. Electronic

polarizability increases both with increasing orbital radius and an increase in the number of orbiting electrons. For isotropic dielectrics in which the polarization is due solely to electron displacement, the dielectric constant is very nearly equal to the square of the index of refraction, n.

$$\epsilon = n^2 \tag{14}$$

Ionic polarizability, a_i, arises from the distortion or displacement of an atom's charge clouds toward stronger binding atoms. The atoms acquire charges of opposing polarities (i.e. ions) which will be displaced relative to an applied field. The magnitude of ionic polarizability is larger for larger ionic radii. Increasing temperature weakens interionic binding forces, thereby increasing polarizability.

The relationship between polarizability and dielectric constant can be explicitly stated by considering the electrical forces from an atomic viewpoint (Kittel, 1976). The local electric field $\mathbf{E}_{loc}$ acting on an atom within a dielectric material is given by:

$$\mathbf{E}_{loc} = \mathbf{E} + \mathbf{E}_L + \mathbf{E}_d \tag{15}$$

where $\mathbf{E}$ is the applied field, $\mathbf{E}_L$ is the Lorentz field due to polarization charges on the inside of the fictitious Lorentz cavity, and $\mathbf{E}_d$ is the dipole field due to permanent dipoles within the Lorentz cavity. For a spherical cavity:

$$\mathbf{E}_{loc} = \mathbf{E} + \mathbf{P}/3\epsilon_o \tag{16}$$

For isotropic media $\mathbf{E}_d = 0$. From equations (12) and (16) one may derive the Clausius Mosotti equation, whereby in materials showing only a_e or a_i, the polarizability can be directly related to the dielectric constant.

$$\frac{\epsilon-1}{\epsilon+2} = \frac{1}{3\epsilon_o} \sum_i n_i \alpha_i \qquad (17)$$

Many molecules are asymmetrically bound yielding a permanent dipole moment. These dipoles, if free to change orientation will tend to align themselves in an electric field, giving a dipolar polarizability, α_d. Under weak applied fields, thermal motion will prevent complete alignment. Therefore increasing temperature will decrease the polarizability of dipolar molecules. α_d is mainly characteristic of polar liquids and gases, and can be observed in semisolid organic materials as well as weakly bonded crystalline solids which have large radicals (e.g. NO_3, TiO_3, SO_4, etc.). Weakly bonded ions displaced from their normal lattice positions by thermal motion may also show a relaxation polarization with behavior similar to that of molecular dipole relaxation.

Material defects, such as grain boundaries, voids, dislocations and impurities can trap charge carriers in the bulk or inhomogeneous material. Such effects can occur with semiconducting and slightly conducting insulators at the electrode-crystal interface. Charges pile up at the electrode and produce a double layer. This barrier layer may result from migration of ions or electrons which cannot leave the dielectric. When a semiconductor is brought into contact with a metal, there is formed in the semiconductor a barrier layer, referred to as the Schottky, or exhaustion layer, from which charge carriers are severely depleted (Kittel, 1976). Upon application of an electric field the random, or layered, inhomogeneities in the dielectric will accumulate charges at the barriers giving the external appearance of an increase in electric permittivity (Maxwell-Wagner effect). These effects are generally referred to as interfacial or surface polarizabilities α_s. Because of α_s, true dielectric constants may be difficult to measure at frequencies below 1 kHz.

In any dielectric the presence and degree of polarizability will strongly depend upon the physiochemical properties of the material as well as the frequency range under consideration. Dielectric constants of most substances show considerable variation with frequency (dispersion). As illustrated in Figure 1 the amount of time required to polarize by displacement or relaxation is inversely related to the frequency at which each polarizability mechanism is influenced.
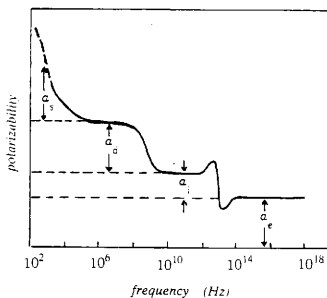
Figure 1. Frequency dependence of the mechanisms contributing to polarizability.

No natural material is a perfect dielectric, but instead exhibits inertial effects and losses. The electrical loss mechanism shows as a phase shift between the applied electric field and the resulting polarization. This loss can be described by a complex electric permittivity:

$$\epsilon^* = \epsilon' - j\epsilon'' \tag{18}$$

The real part ϵ' is a measure of the electrical energy a dielectric can store. The imaginary part ϵ'' or loss factor is a measure of the dissipation of stored electrical energy. More commonly the measured unit is called the loss tangent, $\tan \delta$, defined as:

$$\tan \delta = \epsilon''/\epsilon' \tag{19}$$

When a capacitor is connected to a sinusoidal voltage source V, then:

$$V = V_o e^{j\omega t} \tag{20}$$

where ω is the angular frequency and t is time, the dielectric will increase the capacitance by a factor ϵ/ϵ_o. From equation (3) the charging current (I_c) drawn by the capacitor will be:

$$I_c = dQ/dt = C \ dV/dt = j\omega CV \tag{21}$$

The charging current phase leads the applied voltage by 90°.

If the capacitor leaks any charge, it will also have conductance (G). It will then have a loss current (I_l), which is in phase with the applied voltage:

$$I_l = GV \tag{22}$$

The equivalent electrical circuit containing a leaky capacitor (Figure 2) may be used to represent the dissipation and storage of charge in natural dielectric minerals.
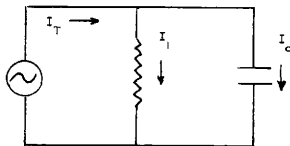
Figure 2. Equivalent electrical circuit for a mineral.

The total current is then:

$$I_T = I_c + I_i = (j\omega C + G) V \tag{23}$$

represented vectorally in Figure 3.
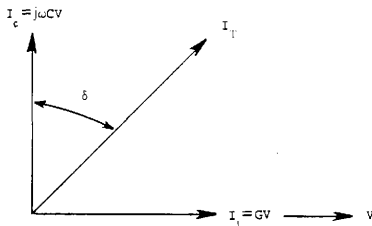
Figure 3. Total current in a lossy dielectric.

Using the complex dielectric constant, equation (23) may be written as

$$I_T = (j\omega\epsilon' + \omega\epsilon'')C_0 V/\epsilon_0 \qquad (24)$$

Neglecting fringe effects, a vacuum capacitor with plate area, A, and separation ,d, has a capacitance value of:

$$C_0 = \epsilon_0 A/d \qquad (25)$$

Since the current density across the capacitor is;

$$J = I_T/A \qquad (26)$$

and the field across the capacitor is:

$$E = V/d \qquad (27)$$

We see from equations (24, 25, 26, and 27) that;

$$J = (j\omega\epsilon' + \omega\epsilon'')E \qquad (28)$$

which is Ohm's law.

Thus by considering the AC conductivity in the dielectric to be $\sigma = \omega\epsilon''$ we can justify using a complex permittivity ϵ^* to take care of all loss mechanisms throughout the AC spectrum.

An alternative way of visualizing the loss angle δ is to look at the relationship of equation (6). When a time varying electric field,

$$E = E_0 e^{j\omega t} \qquad (29)$$

is applied to a dielectric the resulting displacement becomes:

$$D = D_0 e^{j(\omega t - \delta)} \tag{30}$$

where δ represents the phase shift. Therefore, the permittivity is:

$$\epsilon = D_0/E_0 \ (\cos\delta - j\sin\delta) \tag{31}$$

By equation (18), using a complex permittivity we have:

$$\epsilon' = \cos\delta(D_0/E_0) \quad \text{and} \quad \epsilon'' = \sin\delta(D_0/E_0) \tag{32}$$

From equation (32), and by the appropriate identity, we see again that:

$$\delta = \tan^{-1}(\epsilon''/\epsilon') \tag{33}$$

as depicted in Figure 3.

Dielectric measurements on natural minerals have focused on a few minerals of industrial importance, e.g. quartz, tourmaline and mica. For most other minerals, only a few electrical measurements for each have been made, with different techniques at different frequencies and with doubtful accuracy. Also little attention has been given to crystallographic orientation. As a result there may be wide discrepancy for values given by different authors. The problem is further complicated by the fact that minerals are seldom homogeneous. Chemical variations, foreign inclusions, oxidation state etc. will give different results for the same mineral.

The dielectric permittivity of a material is a function not only of the polarizability of the individual particles, but also the number of such particles per unit volume. This parameter is closely related to the density, chemical composition, and crystallographic structure of a material.

CHAPTER III

CHARACTERIZATION OF FERROELECTRIC MINERALS

All minerals belong to one of the 32 crystal classes. Classification is based on axial symmetry. Of these, 20 crystal classes are piezoelectric in that a polarization can be induced by an applied mechanical stress; or conversely, a mechanical strain may result from dipolar realignment due to an applied electric field.

Furthermore, 10 of these crystal classes exhibit an inherent net polarization which exists in the absence of external field stresses. These are known as pyroelectrics, or simply polar classes. The polar classes have a unique polar axis. In other words, the center of positive charge of the crystal does not coincide with the center of negative charge. Such crystals therefore possess a spontaneous polarization, or net electric dipole moment per unit volume.

Frequently the spontaneous polarization cannot be detected by charges on the surface of the crystal because the depolarizing field which results from such a charge distribution can be compensated by the flow of free charges within the crystal and in the surrounding medium (Lines and Glass, 1977). When a crystal having such a structure is heated, the interatomic distances are increased in an asymmetric way. Accompanying such a change in the polar axis is a change in the polarization of the crystal, so the difference in potential is created within. Thus, one can observe the flow of charge to and from the surface. This is the pyroelectric effect. Because conduction currents will obscure displacement currents, direct observation of a pyroelectric effect is often difficult in conducting crystals (Lang, 1974).

A ferroelectric is a crystal possessing spontaneous polarization, which is reversible by application of an electric field. In a ferroelectric crystal two or more

opposing polarization states exist. Referred to as domains, these macroscopic zones form to overcome the depolarizing forces which occur as electronic charges accumulate at the surface of a polar crystal. The application of an external electric field may reorient the permanent dipoles. The phenomenon of reversing the polarization is called the ferroelectric effect (Azaroff, 1975).

The ferroelectric effect can sometimes be demonstrated by observing the dielectric hysteresis loop. In a plot of the polarization (P) vs. applied electric field (E), shown schematically in Figure 4, we see that initially there are an equal number of positive and negative domains. Therefore, the overall polarization is equal to zero. Application of an electric field shows a linear increase in P between O and A. Increasing the field beyond this point results in a nonlinear increase in P until point B. At this point all the domains are oriented in the same direction. Between B and C the crystal is said to be saturated. Now being a single domain, the curve increases linearly. On decreasing the field strength the polarization does not return to zero, but exhibits a remanent polarization OD. Extrapolation of the linear saturation portion back to $E = 0$ will give the value of spontaneous polarization , P_s, represented by OE.

Reversing the field again results in a nonlinear change in P. The value of the field required to reduce P to zero is called the coercive field E_c (OF). Further increase in the field in the negative direction will realign the dipoles in the opposite direction. The relation between P and E is thus represented by the hysteresis loop ($CDGHC$). This is one of the most important characteristics of a ferroelectric crystal.

If the applied field is less than the coercive field, reversal will not occur and the polarization will remain unobservable. Some ferroelectrics have very high coercive fields, and in such cases the field strength required may be greater than
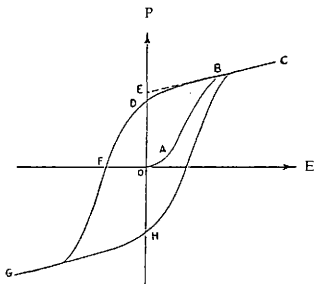
Figure 4. A typical ferroelectric hysteresis loop.

the crystal can accommodate without physical destruction. For materials with high conductivities, e.g. chalcocite, the conduction current obscures the displacement current, and thus it may be impossible to observe the hysteresis directly (Lines and Glass, 1977).

Experimental methods for recording the hysteresis loop are based on the Sawyer-Tower circuit (Sawyer and Tower, 1930) shown in Figure 5. An oscilloscope is normally used to display the hysteresis loop. The horizontal axis depicts the proportional voltage across the crystal. The vertical axis measures the potential across the capacitor in series with the crystal, which is proportional to the charge and; hence, the polarization.
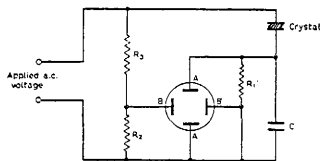
Figure 5. Sawyer-Tower circuit for hysteresis measurement (after Megaw, 1957).

The ferroelectric effect can be illustrated using a simple two dimensional model as shown in Figure 6. There are two possible orientations of the dipoles (domains) in a single pyroelectric crystal.
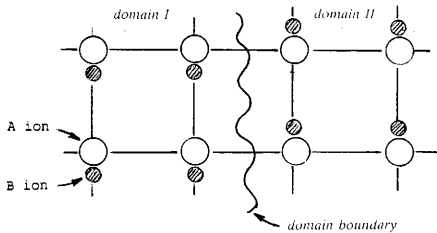
Figure 6. Electrical domains in a hypothetical ferroelectric crystal. Each domain has identical configuration but opposing orientation.

There are two equilibrium positions between the A ions in which the B ions may have the same minimum energy (Figure 7). If sufficient energy is available to overcome the energy barrier ΔE the B ions may go from one minimum equilibrium position to the other.
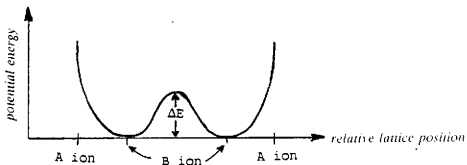
Figure 7. The potential energy barrier between the two dipole orientations.

Applied electric field is not the only factor which effects the dipole in a ferroelectric. If the temperature is sufficiently high, but $< T_c$, the B ions may obtain enough energy to overcome the energy barrier ΔE without the presence of an applied field.

Above a certain temperature, ΔE no longer exists. Therefore there is only one equilibrium position between the A ions (Figure 8). Thus, the crystal will go from a polar to a nonpolar state (Figure 9). The temperature at which this change from polar to nonpolar state takes place is called the Curie temperature, or Curie point. Thermal motion tends to destroy the ferroelectric order. Above the transition temperature, ferroelectricity disappears and the crystal is said to be in a paraelectric state. Almost all ferroelectrics have a Curie point, and those that do not decompose before the Curie temperature is reached. Some ferroelectrics also have a lower transition point, below which they are also paraelectric.
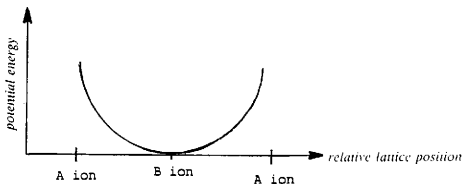
Figure 8. The potential energy between ions in a nonpolar state.
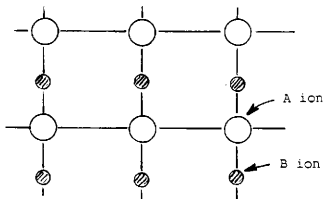
Figure 9. Hypothetical lattice arrangement in the paraelectric state.

As a consequence of atomic shifting that occurs in ferroelectrics, their dielectric properties are quite different from those of non-ferroelectrics. In a ferroelectric the relationship between $\mathbf{D}$ and $\mathbf{E}$ is not linear. The accepted definition of dielectric permittivity for a ferroelectric is:

$$\epsilon = (\partial \mathbf{D}/\partial \mathbf{E})_{E=0} \qquad (34)$$

As the potential between the A ions changes with temperature the polarizability of the B ions changes. The local field produced by the polarization increases at a faster rate than the elastic restoring forces binding the ions in the crystal. Because of this, ϵ also changes with temperature, and will exhibit an anomaly at the transition point (Figure 10). The resulting buildup in the local field's intensity is sometimes called the polarization catastrophe.

The dielectric behavior above the transition temperature is described quite well by the Curie-Weiss law:

$$\epsilon \simeq \epsilon_0 + \frac{\xi}{T-T_c} \qquad (35)$$

Here ϵ_0 is the temperature independent part, ξ is the Curie constant and T_c is the transformation temperature.
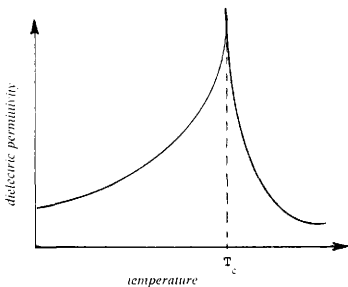
Figure 10. Typical dielectric behavior at the Curie point for a ferroelectric.

A ferroelectric crystal possesses a spontaneous polarization which decreases with increasing temperature, to disappear continuously, or more often discontinuously at the Curie point T_c, as illustrated in Figure 11.
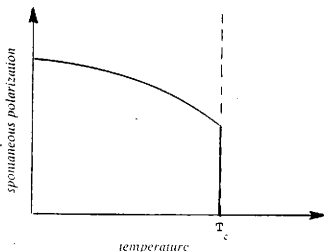
Figure 11. Typical behavior of spontaneous polarization for a ferroelectric.

The electrical conductivity, σ, of a ferroelectric semiconductor (Fridkin, 1980) is related to the concentration of free carriers, n, by:

$$\sigma = qn\mu \tag{36}$$

where q is the magnitude of the charge of the carrier, and μ is the carrier mobility. Both carrier concentration and mobility generally increase as a function of temperature. At the ferroelectric phase transition there is a significant change in carrier concentration. Thus, conductivity anomalies are also characteristic at the Curie point.

One way of demonstrating the ferroelectric effect is by observation of the dielectric hysteresis loop. As was mentioned, for many materials with high

conductivities or very large coercive fields it may be impossible to observe the hysteresis directly. Nevertheless, the dielectric anomaly itself, and its behavior in an applied electric field are very good indicators of ferroelectric phenomena. If a large biasing electric field is applied to the crystal, the Curie point will increase if the transition is ferroelectric, and will decrease if the transition is antiferroelectric (Megaw, 1957).

Polar materials, in particular ferroelectrics, can exhibit a large degree of nonlinearity in their electrical, optical and piezoelectric properties (Burfoot, 1979). Ferroelectric phase transitions are also reflected in specific heat, thermoelectric and dissipation anomalies. Polar dielectric materials characteristically have much higher values of relative dielectric constant. Commonly, ϵ_r is in the range of 10^2 to 10^4 or higher for ferroelectric materials, whereas nonpolar dielectrics usually have ϵ_r between 1 and 10. Large values for ϵ_r are also found in some semiconductors (Parkhomenko, 1971).

Most ferroelectrics have large values of birefringence (Lines and Glass, 1977). Such anisotropy can be attributed to the anisotropy of the crystal structure and electronic polarizabilities (Kinase, 1982). Observation of anisotropy in electrical and optical properties is characteristic in a ferroelectric mineral.

Crystallographic twinning takes place at the transition from higher symmetry to lower symmetry. Mimetic twinning in minerals is caused by the necessity of stability of an orientation state (i.e. domain) which is governed by the Gibbs free energy function G. For two neighboring domains, a and b, to be in thermodynamic equilibrium, G_a must equal G_b. To minimize ΔG (ideally 0) there is an orientation state shift (Newnham, 1974). In ferroelectrics $\Delta G \simeq \Delta P$ (i.e.- difference in spontaneous polarization between domains).

Ferroelectric domains are often visible in polarized light. Therefore, the presence of domain structure is an important indication for classifying a substance as a possible ferroelectric (Zheludev and Sonin, 1958).

Ferroelectric crystals may be divided into two main groups based on their structural changes. In order-disorder ferroelectrics, the transition is associated with the individual ordering of ions. In displacive ferroelectrics, the transition is associated with the displacement of a whole sublattice of ions of one type relative to another sublattice.

Structural transitions may also be defined as first order or second order, depending upon whether the change in polarization and thermodynamic state at the transition takes place discontinuously or continuously. Ferroelectric phase transitions may be of either type. Most ferroelectrics have first order transitions.

In contrast to ferroelectrics, antiferroelectrics are characterized by an antipolar arrangement of the atoms in the crystal lattice, which yields a zero net dipole moment (Figure 12). Therefore, no dielectric hysteresis loop can be observed below the Curie temperature (Jona and Shirane, 1962). Antiferroelectrics do have very high dielectric constants, as in ferroelectrics, and will also show a dielectric anomaly at the transition point.

Antiferroelectrics will typically reveal a lattice transformation from a substructure to a superstructure containing a multiple of substructure units (usually two times the cell perpendicular to the polar axis) when becoming antiferroelectric. This doubling is to accommodate the lattice segments of opposing polarity.

The antipolar character of a crystal can be established by X-ray diffraction methods, but only dielectric measurements can definitely establish its antiferroelectric character (Jona and Shirane, 1962).
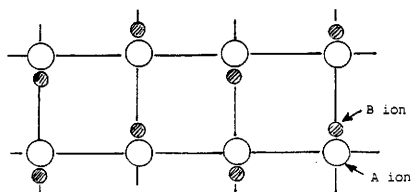
Figure 12. The antipolar arrangement of dipoles in an antiferroelectric crystal.

CHAPTER IV

THE PHYSICAL PROPERTIES OF CHALCOCITE

Crystallography and Mineralogy

Chalcocite, Cu_2S, is one of the most important copper ore minerals. It occurs primarily in supergene enrichment zones as a massive "blanket" deposit (Park and MacDiarmid, 1975). Chalcocite is also common as a primary hydrothermal sulfide, and in reduced sediments (Shuey, 1975). Chalcocite is found mainly as a fine grained polycrystalline mass, often with some proportion of djurleite ($Cu_{1.96}S$) and digenite ($Cu_{1.8}S$). Crystals are very rare, usually small, having an elongated prismatic habit or a tabular habit with hexagonal outline (Figure 13) and are commonly striated parallel to the a axis (Hurlbut, 1971). Twinning is prevalent, with very fine domains sometimes visible under transmitted or reflected light.
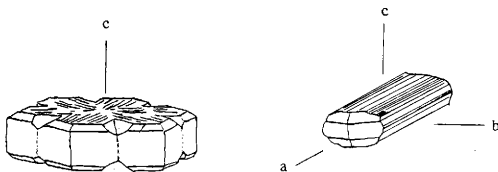
Figure 13. Chalcocite crystals. (a) pseudohexagonal twins (after Sinkarikas, 1966) (b) prismatic habit (after Hurlbut, 1971).

Chalcocite is easily identifiable by its gross mineralogical properties. Natural specimens are shiny lead grey in color with metallic luster, tarnishing to dull or sooty black on exposure to air. Chalcocite has a hardness of 2.5-3, and a specific gravity of 5.5-5.8. It exhibits poor cleavage on the 110 plane and shows conchoidal fracture when broken.

With X-ray diffraction, Buerger and Buerger (1944) verified a structural transformation of Cu_2S at 105°C from orthorhombic, space group $Abm2$ (C_{2V}^{15}), to hexagonal, space group $P6_3/mmc$ (D_{6h}^4). Djurle (1958) confirmed the work of Buerger and Buerger, showed with Weisenberg photographs that low temperature chalcocite had an A-centered orthorhombic unit cell containing 96 Cu_2S (Figure 14). The unit cell dimensions were determined to be:

$$a = 1.1881 \text{ nm} \quad b = 2.7323 \text{ nm} \quad c = 1.3491 \text{ nm}$$

Djurle also showed the transition at 105°C to the hexagonal structure and another transition at 470°C to a face-centered cubic lattice.

Evans (1971, 1979, 1981) redetermined the low temperature phase to be monoclinic, space group $P2_1/c$ (C_{2h}^5) with the unit cell containing 48 Cu_2S (Figure 15). This space group implies that the chalcocite crystal structure is centrosymmetric in its low temperature, as well as the high temperature phases. However, Evans (1979) further states that it is an asymmetric unit due to the fact that several of the Cu^+ ions may each equally well lie in two possible sites. Since the chalcocite structure below 105°C shows no disorder, random switching of sites is not probable. Evans (1971) has shown that the pseudo-orthorhombic aspect of the X-ray diffraction effects from most crystals is due to fine scale twinning on the monoclinic (100) plane. Many researchers still refer to the structure of low temperature chalcocite as orthorhombic or pseudo-orthorhombic. More detailed crystal studies are required to resolve the remaining discrepancies.
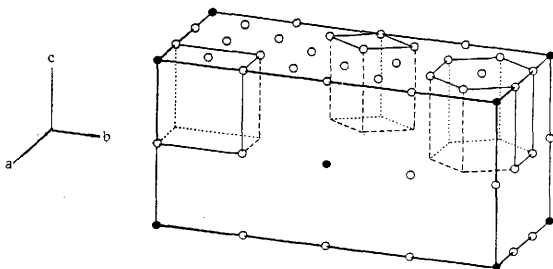
Figure 14. The A-centered orthorhombic low chalcocite cell. Dashed lines outline three kinds of high chalcocite cells. The black dots are lattice points of low chalcocite, the open dots are lattice points of high chalcocite (after Buerger and Buerger, 1944).

$Cu_{1.96}S$ was first identified as a separate phase by Djurle (1958). Takeda and others (1967a, 1967b) investigated the crystallography and twinning of Djurleite, finding the structure to also be either orthorhombic or monoclinic. Evans (1979, 1981) has shown that djurleite is indeed monoclinic, space group $P2_1/n$, with an asymmetric structure similar to, but even more complex than chalcocite.

X-ray work by Evans (1981) shows that all the copper atoms are in triangular coordination with sulfur atoms. Some are fairly regular in their bonding while others show quite severe distortion in the triangle. One Cu atom is displaced strongly from the triangular plane towards a tetrahedral site. Both chalcocite and djurleite have a continuous Cu-S net that is interrupted in an ordered manner by many vacant triangular sites.
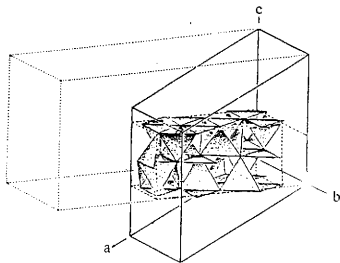
Figure 15. Monoclinic unit cell for low chalcocite. Triangles represent CuS$_3$ groups, of which those corresponding to a little more than one asymmetric unit (indicated by dashed lines) are shown. The dotted lines indicate the end-centered orthorhombic pseudocell (after Evans, 1979).

The copper-sulfur bond lengths in chalcocite and djurleite vary from 0.22 nm to 0.29 nm (Evans, 1981). Sorokin (1966) has shown that the current carriers in polycrystalline chalcocite are mainly scattered by acoustic lattice vibrations (phonons). Therefore the dominant bond type is covalent, as would be expected if inferred from the difference between the electronegativities of copper and sulfur ions. Ionic bonding in chalcocite, although probably less than 40% of the total bonding (Sorokin, 1966), may be very important in the manifestation of its physical properties.

Phase Relationships

The Cu-S system (Figure 16) has been extensively studied by Roseboom (1966) and Cook (1972). Cuprous sulfide in nonstoichiometric proportions exists as djurleite ($Cu_{1.96}S$) and digenite ($Cu_{1.8}S$). All of these phases undergo one or more transitions at higher temperatures. Djurleite has a transition at 91°C from monoclinic to hexagonal. Each ultimately transforms into a face centered cubic phase. Jensen (1947) determined the melting point of Cu_2S to be near 1130°C. Chalcocite and djurleite represent low temperature superstructures of the same high temperature disordered chalcocite subcell. The djurleite superstructure is the more stable form at room temperature (Putnis, 1977).

A metastable tetragonal phase with composition $Cu_{1.96}S$ exists between 94°C and 146°C. First described by Djurle (1958), this phase appears to be a high temperature modification of djurleite. Janosi (1964) concluded from powder X-ray diffraction that the tetragonal structure was one of closest cubic packing, but slightly deformed. The space group $P4_3 2$ was determined. The stability of the tetragonal form at atmospheric pressure is debatable (Skinner, 1970). Serebryanaya (1966) and Roseboom (1966) conclude that the tetragonal Cu_2S may be preserved at room temperature and atmospheric pressure, but not indefinitely. At 146°C this phase also transforms to the face centered cubic lattice.

Complications from this tetragonal phase are not likely since, as Cook (1972) points out, the transformation is very sluggish. All compositions between Cu_2S and $Cu_{1.96}S$ transform completely to tetragonal, but several months are required for complete conversion at temperatures between 94°C and 120°C. Exposed to air, chalcocite will slowly convert to djurleite (Cook and others, 1970). Therefore, most chalcocite specimens are probably not stoichiometric Cu_2S. However, Kazinets and others (1979) reported that heating in a vacuum or inert atmosphere
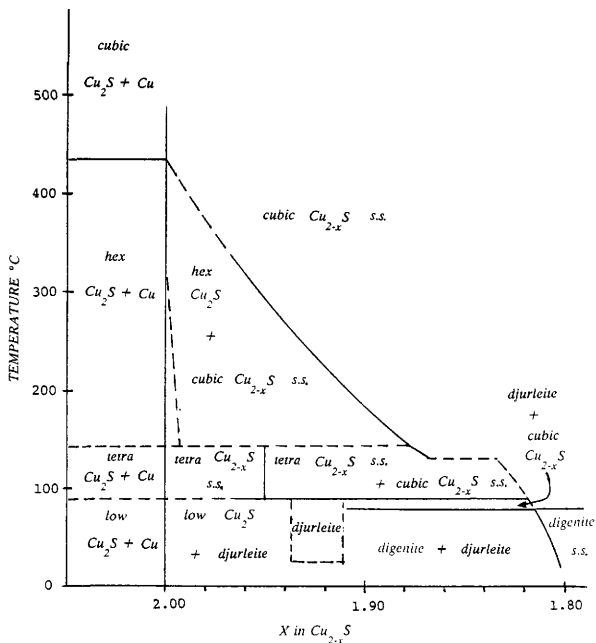
Figure 16. Phase diagram for Cu-S system. For compositions between 0°C and 500°C. Abbreviations: hex - hexagonal, tetra - tetragonal, low - orthorhombic(monoclinic), s.s. - solid solution (after Cook, 1972).

will eventually convert digenite and djurleite back to chalcocite, as a result of the volatilization of sulfur.

Chen and Chang (1974) investigated the silver-copper-bismuth sulfide and silver-copper-antimony sulfide phase systems. All the end members can co-exist with various solid solution phases consisting of various amounts of the other members. Many of these sulfides have similar structures and similar physical properties. Low temperature phase transformations are common. Bismuthinite, Bi_2S_3, and stibnite, Sb_2S_3, are known to be ferroelectric (Lines and Glass, 1977). The possibility that other chemically and structurally related compounds would also exhibit ferroelectric behavior has been suggested by Corry (1984).

Electrical Properties

Chalcocite is known as a good but variable conductor. Chalcocite is a p-type semiconductor (Shuey, 1975) in which copper vacancies act as acceptors. Hence, the electrical conductivity of this substance depends strongly upon the deficit amount of copper atoms in the specimen (Okamoto and Kawai, 1973).

Electrical conductivity at room temperature increases with increasing copper deficiency. Stoichiometric Cu_2S has a room temperature resistivity of 10^4 Ω-m (Wagner and others, 1982), but decreases by five orders of magnitude for $Cu_{1.8}S$. Materials with resistances as low as 10^5 Ω-m are still considered dielectric (i.e. - insulators) although somewhat "lossy" (Shuey, 1975).

Above the transition temperature of 105°C, the copper ions appear to be quite mobile within the hexagonal sulfur lattice. Thus, in this phase, ionic conductivity is prevalent and increases exponentially with increased temperature, and is essentially independent of composition (Okamoto and Kawai, 1973). Due to cation ordering, ionic conductivity is not found in the low temperature phase

where hole conductivity predominates.

The Hall effect in chalcocite was measured by Hirahara (1951b) and Abdullaev and others (1968). They noted that conductivity showed only a minor increase with temperature up to the phase transition, characteristic of semiconductors. At the transition, a 4 to 7 fold drop in hole mobility is observed presumably due to scattering from the cation disorder. Okamoto and Kawai (1973) showed that the phase transition of nearly stoichiometric Cu_2S is observed quite distinctly, especially in the cooling cycle. After the transition, carrier mobility tends to decrease slowly until near 400°C, where semiconductor effects again give rise to a rapid increase in conductivity. Measurements of thermo-emf by Hirahara (1951a) show a steady increase with a significant jump at the transition point. Carrier concentration, likewise, decreases with increasing stoichiometry and shows a drop at the transition.

A great deal of work has been done on the use and characteristics of Cu_2S in photoelectric devices (Arjona and others, 1979, Duchemin and Gaustavino, 1978). Recognized as the essential phase in Cd/Cu_2S type solar cells, development has been hampered by insufficient knowledge of its microstructure, thermal stability, optical and electrical properties (Arjona and others, 1979). Rothwarf (1980) has investigated the operation of this type of high energy solar cell and notes anomalous effects which have not been completely explained.

The conduction band presumably derives from the Cu 4s level, while the valence band must be based on the Cu 4d and S 3p levels (Shuey, 1975). Only minimal research has been done on band calculations in Cu_2S. It appears there are two edges. One edge has been calculated to be at 1.2 eV (Marshall and Mitra, 1965, Abdullaev, 1968). The other band edge occuring in the range of 1.7 to 2.5 eV (Mulder, 1973b). Mulder (1973b) suggests a band model with two types of

transitions, an indirect at 1.2 eV and a direct at 2-2.5 eV. Anisotropy in the indirect band was found in single crystals, although only the direct energy transition appears to be effected by the phase change at 105°C.

Ibragimov and others (1979, 1982) investigated the influence of uniaxial deformation on the electrophysical properties of polycrystalline and single crystal Cu_2S vs. temperature. Under a given load they observed a decrease in electrical conductivity and pressure coefficient at the phase transition.

An extensive literature search has shown no experimental work concerning the dielectric properties of Cu_2S. Povarennykh (1960) deduced that the dielectric permittivity for ionic covalent bonded minerals increases with increasing atomic weight, degree of covalency, the coordination number, and the number of free electrons but decreases with interatomic spacing (Parkhomenko, 1967). The predicted value for the relative dielectric constant of chalcocite, arrived at by Povarennykh, is > 81.

Magnetic Properties

Adou and Baudet (1967) examined the magnetic susceptibility of Cu_2S over a large temperature range. They concluded that chalcocite was diamagnetic and that within the sensitivity of their instrumentation the magnetic susceptibility was essentially independent of temperature. However, a small drop in susceptibility was recorded in the region of the phase transition. The change in susceptibility at the transition became more pronounced with increasing nonstoichiometry.

Optical Properties

Optical anisotropism is weak, but very distinct when uncrossing the nicols. Characteristic orange brown or dark green tints are apparent (Picot and Johan, 1982). The red brown crystals are weakly doubly refracting with a dull yellow color. Transition to hexagonal form in is visible in transmitted light as a reversible darkening at 105°C often with transient buckling (Mulder, 1972). The absorption of light is most favorable for light polarized perpendicular to the c-axis (Mulder, 1973a). Birefringence and domain structure is also evident in djurleite, but not in digenite which is isotropic (Mulder, 1972). At 105°C Mulder (1973b) noticed a small discontinuous increase in absorption at higher spectral energies.

Mulder (1973b) shows the index of refraction of chalcocite to be $\simeq 3$. If chalcocite was considered to be isotropic then, by equation (14): $\epsilon_r \simeq n^2 \simeq 9$.

Although still fairly high for a dielectric constant it is much less than the value of >81 arrived at by Povarennykh (1960). Thus, there must be a large contribution to polarizability from the ions, free electrons and possibly permanent dipoles.

Thermodynamic Properties

The chalcocite phase transformation is reflected in specific heat, thermoelectric and heat capacity anomalies (Ueda, 1949, Hirahara, 1951a, Abdullaev and others, 1968). A small decrease in density and, conversely, a small increase in molar volume has been observed in the transition from low chalcocite to hexagonal chalcocite (Clark, 1966). Ueda (1949) showed that there is a considerable change in the lattice constants at the transition point, but without discontinuity.

The hexagonal orthorhombic transition is rapid, but will show a 10-15° hysteresis (Cook,1972). This thermal hysteresis in quite marked and is noted in every investigation of the physical properties at the transition. Arjona and others (1979) suggests that this is due to a nucleation process.

The enthalpy of transformation, ΔH, was calculated by Hirahara (1951a) and again by Arjona and others (1979) and found to be indicative of first order transition. Differential thermal analysis shows distinct endothermic peak at 105°C (Smykatz-Kloss, 1974). Jost and Kubaschewski (1968) thoroughly investigated the specific heat from -70°C to 550°C. Their studies show very sharp anomalies at 105° and 440°C. Luquet and others (1972) showed by differential thermal analysis that for compositions between $Cu_{1.96}S$ to almost stoichiometric Cu_2S a third anomaly occuring around 175°C. The anomaly was attributed to the tetragonal phase transition.

Ferroelectric Properties

On the basis of crystal symmetry relationships between the low temperature phase and the hexagonal phase, Zheludev and Sonin (1958) predicted ferroelectricity in Cu_2S. No further research on this aspect has been published, to my knowledge. Parkhomenko (1971) listed chalcocite as a piezoelectric and pyroelectric mineral, although no references were given.

Ferroelectricity in chalcocite appears probable as strongly suggested by its established physical properties. Cu_2S has a structurally ordered low temperature phase which is fairly complex and asymmetric. Chalcocite has a phase transition to a very disordered centrosymmetric structure at 105°C. Anomalous behavior in conductivity, thermodynamic and optical properties have been observed at the transition point. Birefringence is indicative of crystalline anisotropy. The atomic

bonding, crystallographic structure, and semiconducting nature of Cu_2S may imply a high dielectric permittivity.

Antiferroelectric behavior in low chalcocite should also be considered. In X-ray diffraction studies of the Cu_2S transformation, Putnis (1977) observed that just below the transition, a $2a \times 1c$ cell pattern is distinctly observed, characteristic of paraelectric to antiferroelectric phase transitions. On further cooling the superstructure reflections corresponding to either chalcocite of djurleite appear.

CHAPTER V

EXPERIMENTAL TECHNIQUES, EQUIPMENT AND PROCEDURES

To characterize chalcocite as a possible ferroelectric it is essential to demonstrate that the dielectric behavior of chalcocite is nonlinear as a function of temperature and as a function of applied electric field. Furthermore, anomalous behavior in both dielectric permittivity and conductivity is expected at the Curie temperature, provided chalcocite is ferroelectric.

Experimental Techniques and Equipment

The principal method for determining the real and imaginary parts of the dielectric constant is the comparison of the capacitance of an empty capacitor C_o with that same capacitor containing the dielectric material C. From equation (1) and (25), the capacitance of a dielectric, with electrode area, A, and thickness, d, is:

$$C = \epsilon_r \epsilon_o A/d \tag{37}$$

Therefore, the dielectric constant is directly related to capacitance divided by the permittivity of free space times the ratio of electrode separation to electrode area.

$$\epsilon_r = C(d/\epsilon_o A) \tag{38}$$

ϵ_r of course, is the magnitude of both the real and imaginary parts of the relative dielectric constant. For dielectric materials with very low conductivity, the contribution from ϵ'' is negligible and therefore, $\epsilon_r \simeq \epsilon'$. For more conductive materials, ϵ'' will be significant, particularly at low frequencies.

Capacitance is typically measured with an LCR bridge (Inductance-Capacitance-Resistance). When using an LCR bridge (e.g. General Radio model #1650-A), the unknown material is compared with standard inductances and capacitances built into the bridge. Detailed discussions on the construction and operation of various bridge configurations can be found in standard texts (e.g. Loeb, 1967, Starling, 1947).

In modern electronic bridges (e.g. Electro-Scientific Industry model #353 Impedancemeter or ESI model #296 Auto LCR Meter) a constant voltage at a controlled frequency is applied across the unknown to be measured. Phase sensitive detectors separate the in-phase (0°) or quadrature (90°) component with respect to the input reference voltage. The ratio of the output voltage to input voltage is then directly converted to capacitance or conductance.

Standard techniques for measuring capacitance do not work with semiconductor or metallic conductors. In such materials, free charge carriers can prevent polarization charges from accumulating at the electrode surfaces. Furthermore, Maxwell-Wagner effects and Schottky barriers may produce anomalously high and variable capacitances. With large numbers of free carriers there is usually some amount of inductance (L). The series capacitance (C_s) (i.e. capacitance measured with a constant applied current) can be simply related to the inductance and resistance (R) by:

$$C_s = \left((2\pi f)^2 L + R^2/4L \right)^{-1} \tag{39}$$

The series capacitance is related to the parallel capacitance (C_p), (i.e. normal mode for measuring capacitance; measured with applied voltage constant) by the dissipation factor or loss tangent (tan δ).

$$C_s = (1+\tan^2\delta)C_p \qquad (40)$$

In materials with low loss then, $C_s \simeq C_p$. As the loss becomes larger this relationship becomes important when trying to measure electric permittivities.

Alternatively, separation of phases may also be done using a Lock-In Amplifier (e.g. EG&G model #5101). To determine the conductance or capacitance of the unknown material, a reference imput voltage (V_{in}), frequency (f), and phase (0° or 90°) is selected. Only those signals which are synchronous with the reference are converted to a dc output voltage (V_{out}). The following simple relations are used to calculate the capacitance or conductance. 'Sens' is the total sensitivity factor or input signal level range selected on the Lock-In Amplifier.

$$C = V_{out}(sens)/2\pi f V_{in} \qquad (41)$$

$$G = V_{out}(sens)/V_{in} \qquad (42)$$

The accurate determination of ϵ depends upon the technique used, the quality of instrumentation and sample preparation, and ultimately the composition and homogeneity of the sample itself.

Sample Description and Preparation

In order to make dielectric measurements on chalcocite, mineral specimens had to be prepared as a parallel plate capacitor. Most of the work was done using polycrystalline bulk samples, as commonly found in chalcocite "blanket" deposits in southwestern U.S. The bulk chalcocite samples were obtained from the mineralogical collection of the Texas A&M Department of Geology. The high-grade specimens are assumed to have come from Arizona or Montana. The

"thumb-nail" sized specimens were coal black in color with no visible evidence of alteration. The cut surfaces were typically shiny lead grey and macroscopically uniform.

Several single crystal samples from Butte, Montana were purchased through Ward's Scientific Supply Co. (Rochester, N.Y.). The specimens were tabular shaped with dimensions of 2mm x 5mm x 10mm. The "brassy" surfaces were tarnished and striated along the longest face. A pseudohexagonal outline is evident in the single crystal samples. Pseudomorphism of crystals indicates thermal conditions at the time of formation (Vaughan and Craig, 1978). This suggests that the chalcocite was formed by hydrothermal cooling through the transition temperature. The Butte, Montana mineral district is rich in gold, silver, lead, zinc, arsenic, molybdenum and iron. Small quatities of these elements are possibly present as impurities in the chalcocite samples tested. Single crystal research is hampered by the rarity of good quality large crystals. Because of the softness and fragility of chalcocite, thin slices were difficult to obtain.

Samples were cut on parallel faces using a low speed diamond wheel saw (South Bay Tech. model #650). The thin specimens were polished with 600 grit silicon carbide paper (Wetordry Tri-m-ite by 3m company) using a Buehler Ecomet III Grinder/Polisher. The finished samples had thicknesses on the order of 1mm and with a surface area of approximately 1 cm^2 (single crystal samples were smaller). Single crystal samples were oriented parallel or perpendicular to the c-axis based on external crystal morphology (see Figure 13). Prepared samples were boiled in acetone prior to applying electrodes to remove any contaminants on the surface from handling and polishing. To form the electrodes, silver paint (Silver Print Conductive Paint made by GC Electronics, Rockford, Ill.) was carefully applied with a brush to two parallel sides. The silver paint was dried at

approximately 75° C for 10 to 24 hours using an infrared lamp. Thorough drying is important to remove residual volatiles (the silver paint had a butyl acetate base).

The silver electrodes were visually inspected before each experiment. Usually, after several successive heating-cooling cycles the electrode surfaces were repolished or reapplied if necessary. Deterioration of the silver electrodes seemed to occur if the sample surface had not been cleaned sufficiently to insure good adherence of the paint. Insufficient drying time after electrode application resulted in the paint sticking to the copper sample holder. The electrode would then peel or flake off when the sample was removed.

<center>Experimental Procedures</center>

The chalcocite samples were mounted in the sample holder (Figure 17). A spring loaded copper rod insured good constant electrical contact to the silver electrodes during heating and cooling.

The Lock-In Amplifier or the LCR meter was connected via coaxial cables to the copper electrode leads. Periodic readings were recorded by hand from the digital readouts. Simultaneously, curves were traced by analog output to an X-Y recorder (Figure 18).

The sample chamber was first evacuated, then filled with argon or nitrogen atmosphere. The chamber was kept at slightly positive pressure to guard against atmospheric contamination and sample oxidation. The importance of using an inert atmosphere, or vacuum, when heating Cu_2S was noted very early in experiments by Buerger (1941). When heated in contact with air, copper sulfide oxidizes and Cu_2S will begin to convert to digenite, $Cu_{1.8}S$.

The sealed sample chamber was placed in a small furnace. The heating rate was kept roughly linear by controlling the voltage and current applied to the furnace. The approximate heating rates vs. applied voltages were determined for the furnace prior to the experiments. Initially the furnace was allowed to cool at its own rate. However, this resulted in a cooling rate several times faster than the heating rate.

More carefully controlled heating and cooling was done with a microprocessor controller. With the controller, both heating and cooling rate could be precisely set. However, a heating or cooling rate of less than 1°C per minute could not be accurately achieved with the system used in these experiments. Most of the experiments were run with a heating rate on the order of 100° to 150°C per hour.

Observation of a ferroelectric hysteresis loop was attempted using the method described in Chapter III.
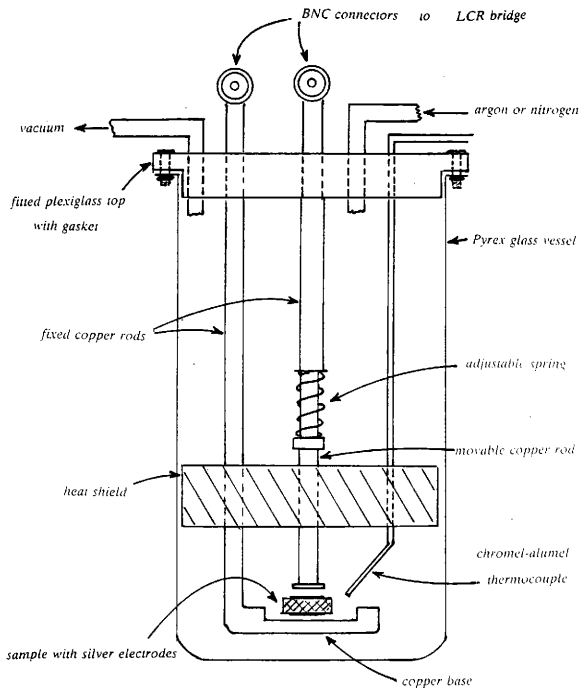
Figure 17. Sample holder used for measurements in the range of 25°C to 225°C.
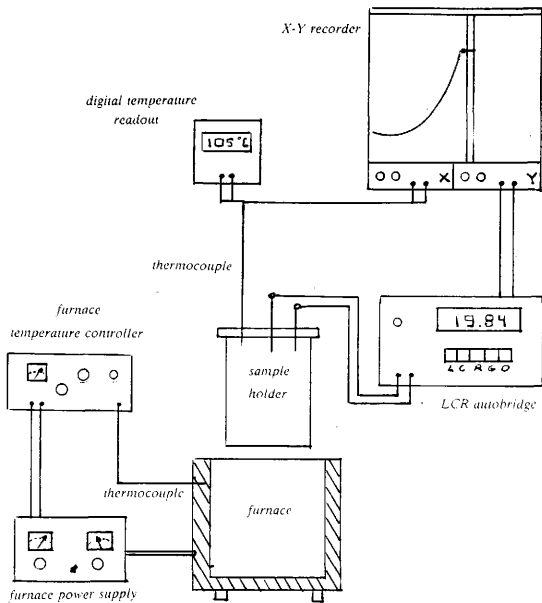
Figure 18. System used for measuring the electrical properties as a function of temperature.

CHAPTER VI

RESULTS AND DISCUSSION

Electrical Conductivity of Chalcocite

The electrical conductivity of the chalcocite specimens were easily determined. The conductance, G, was measured directly with an ESI model # 253 Impedancemeter. The conductivity (σ) is simply related to the conductance, sample thickness (d) and sample cross-sectional area (A) by:

$$\sigma = G \ d/A \tag{43}$$

The room temperature conductivities at 1 kHz are found in Table 1. AC conductivity is measured rather than dc conductivity because the dc field does not address the responses due to dipole rotation, which is important in ferroelectrics.

Table 1. Electrical conductivities of the chalcocite samples at 1 kHz.

Sample	Conductivity in S/m
polycrystalline #1	1.34
polycrystalline #2	9.63
single crystal ‖ C	720
single crystal ⊥ C	38.3

The range of conductivity for chalcocite varies considerably in the literature, which again illustrates the variations from sample to sample and the techniques for measurement. The values for the specimens used in this study are within the range of literature values. The lower conductivity in the polycrystalline material is probably due to more impurities and bulk imperfections than are present in the single crystal samples (also by no means perfect).

Okamoto and Kawai (1973) found that the conductivity varied from 7 S/m to 2.4 x 10^5 S/m as the deviation from stoichiometry increased from Cu_2S to $Cu_{1.8}S$. They also noted that the transition temperature of Cu_2S increased from 98°C to 108°C as the conductivity decreased from 5.20 x 10^3 S/m to 7 S/m. These measurements were made on grown polycrystalline material. Typically in a semiconducting ferroelectric, a decrease in the Curie point with increase in free carrier concentration is observed (Lines and Glass, 1977). Therefore, such behavior in chalcocite would indicate that even though there is a structural difference between the Cu_2S and $Cu_{1.96}S$ phases the causative ferroelectric mechanism is inherently present.

For grown polycrystalline digenite, Kamigaichi (1952) found a conductivity range of 1.4 x 10^2 S/m to 2.0 x 10^6 S/m. The lower conductivity value is close to that for stoichiometric djurleite. On the bases of conductivity then, it can be assumed that there is little digenite, if any, in the specimens tested.

Abdullaev and others (1968) worked with grown single crystals of chalcocite. They found room temperature conductivity to be in the range of 1.7 x 10^4 S/m. However, there was no reference to crystallographic orientation.

Anisotropy in the conductivity of single crystals of Cu_2S has not been reported in the literature. The thin tabular habit of single crystals makes electrical measurements in axes other than the c-axis very difficult. Once a sample is cut

along a specific plane, any perpendicular direction has insufficient surface area to thickness ratio to work with (at least with the methods used in this study). Therefore, although a large difference in conductivity was noted here for the sample measured ∥ to c-axis and for the sample measured ⊥ to the c-axis, true anisotropy could not be adequately demonstrated.

The behavior of the conductivity of chalcocite at its transition at 105°C has been studied by several researchers. Hirahara (1951a) states the conductivity in chalcocite single crystals increases according to an exponential law, with the temperature increase from room temperature, which behavior is characteristic for semiconductor. At about 110°C however, the electrical conductivity drops suddenly and then increases gradually with temperature.

Although not as clear in the polycrystalline samples measured here (Figures 19 and 20), this behavior was clearly noted in the single crystal sample shown in Figure 21. Hirahara (1951a) also noted that there was a significant contribution to the total conductivity by ionic conductivity which was observed above 150 °C. It is possible he may have also been observing the tetragonal phase transition.

In polycrystalline sample #1, the transition temperature (e.g. Figure 19) was found to occur between 125°C to 150°C on heating, and usually 10-20° lower on cooling. The main reason for the high transition point in my initial experiments was bad placement of the thermocouple. The thermocouple was repositioned much closer to the sample for later experiments. The transition point was then observed to occur between 100° to 120°C. Deviation from the established transition temperature of 105°C can be attributed to non-uniform, or to a too fast rate of heating. On cooling, the large characteristic anomaly in both conductivity and permittivity always occured between 95°C and 110°C, as seen in Figures 20, 21 and 22. Therefore, it was concluded that the anomalies observed during the

cooling cycle are due to the transition from from high chalcocite to low chalcocite. The large thermal hysteresis between heating and cooling cycles is due to relaxation inherent in chalcocite, i.e. the electrical response mechanisms are not the same for heating as cooling.

Another peak was observed to occur approximately 40° to 60° above the first transition point (e.g. see Figures 21 and 22). Although small, this anomaly has a characteristic shape of a ferroelectric transition. It is possible that this transition is due to the presence of some amount of the tetragonal phase, which undergoes a phase transition at about 145°C. In cooling, some samples inconsistently showed a broad anomaly between 40° to 80° (Figure 22). This may also be due to the sluggish transformation of the tetragonal phase or perhaps the presence of some other impurities.

Some ferroelectrics do undergo several phase transitions. Each successive phase being ferroelectric until the paraelectric state is reached. Barium titanate, which is one of the most studied ferroelectric materials, exhibits such behavior. It has a transition at -90°C from a rhombohedral to a orthorhombic phase and a transition at 5°C to a tetragonal phase, all of which are ferroelectric, and then ultimately undergoes a transition to a cubic paraelectric phase at 125°C (see page 64). Perhaps the multiple phase transitions in chalcocite reflect a similar behavior.
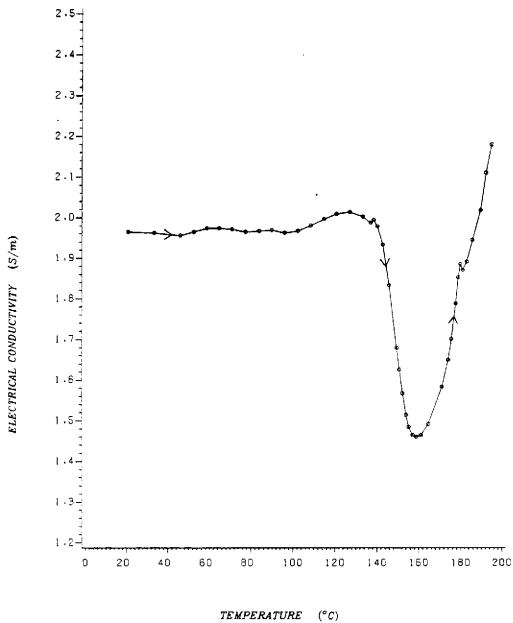
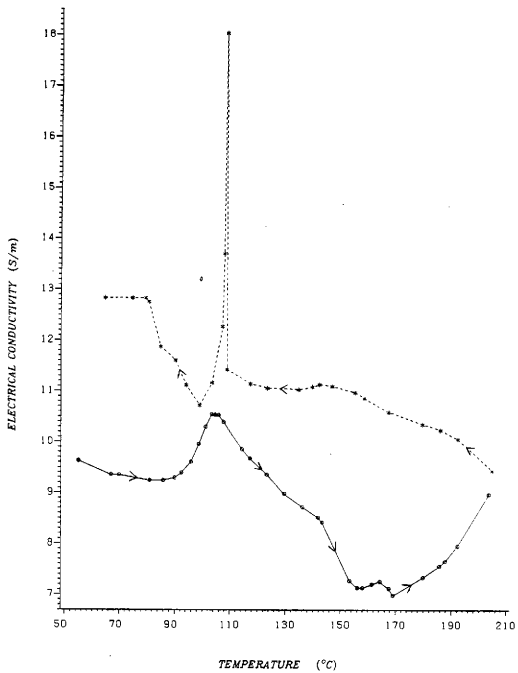Figure 19. Electrical conductivity behavior in polycrystalline sample #1 at 1 kHz.

Figure 20. Electrical conductivity behavior in polycrystalline sample #2 at 1 kHz.
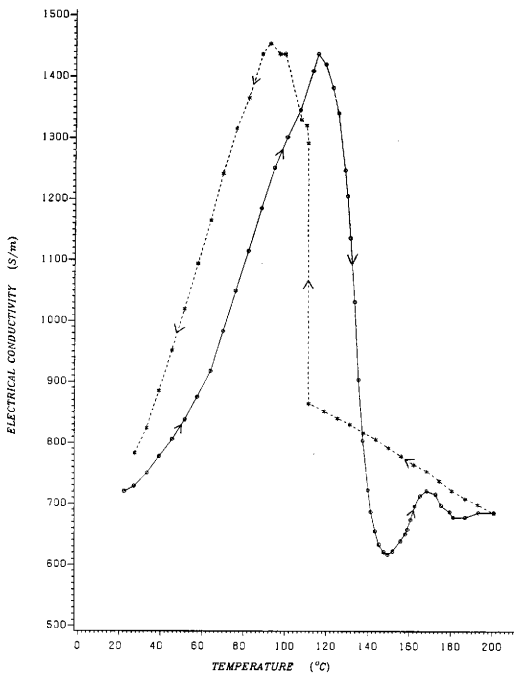
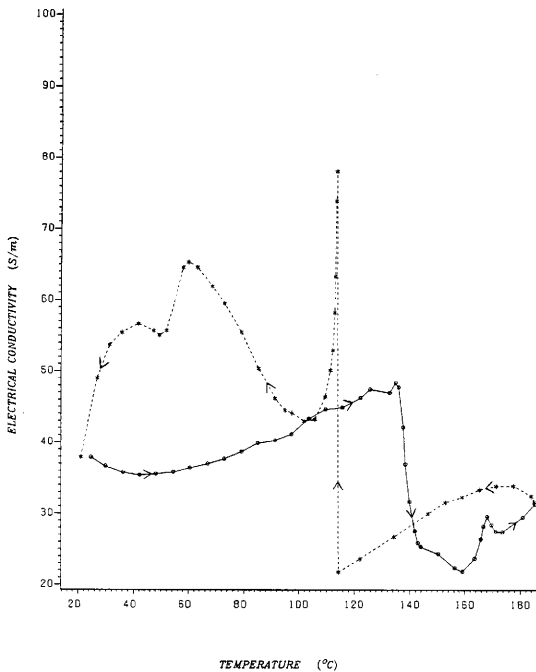Figure 21. Electrical conductivity behavior in single crystal ‖ to c-axis at 1 kHz.

Figure 22. Electrical conductivity behavior in single crystal ⊥ to c-axis at 1 kHz.

Dielectric Constant of Chalcocite

Attempts were made to measure the dielectric constant for chalcocite. Assuming chalcocite to be a low loss material, then by equation (37) the expected range of capacitance for the parallel plate samples could be estimated.

For a conservative value of $\epsilon_r = 10$, the single crystal specimen would have a capacitance: $C = \epsilon_r \epsilon_o \, (A/d) \simeq 10 \times (8.85 \times 10^{-12}) \times .0279 \simeq 2.47 \times 10^{-12}$ F.

This is a very small value, on the order of the capacitance value of the sample holder itself (see appendix A) and also below the variation and drift due to the electrode contacts, wire connections and meter calibrations.

A much larger value for ϵ_r of 10^4 would give a calculated capacitance in the range of 2.5×10^{-9} F. This range is easily measured on most bridges provided there is a good signal to noise ratio.

Direct measurement of capacitance with the standard bridge (General Radio model #1650-A) failed to give any value. The ESI Auto LCR Meter and Impedancemeter also failed to give any believable values. The Auto LCR Meter would give values in the negative 2 - 3 μF range. The reason for the negative sign is not fully understood. Ignoring the negative sign, dielectric permittivity values calculated to be in the range of 10^7, which is unrealistically high for any ferroelectric, let alone one with high conductivity. Free carriers, Maxwell-Wagner effects and Schottky barriers may well be responsible for these results at low frequencies.

The ESI instruction manual mentions that if a negative sign occurs when measuring capacitance it may be that the unknown being measured is inductive. Furthermore negative signs may be expected when measuring electrolytic capacitors or semiconductors which require biasing.

Application of a small DC bias voltage (<1V) to the sample via the internal circuitry of the Auto LCR Meter did give positive capacitance values in the range of 0 to 20 μF. However, the capacitance varied with the strength of the applied bias voltage, generally increasing up to a point and then returning to negative value. A maximum voltage to stabilize the capacitance could not be determined because the instrument's bias input is current limited to 0.1A, which is quickly reached due to the low resistance of the sample. In comparison, application of the same DC bias to a standard capacitor (several were tried in the range of $10\rho F$ to $10\mu F$) did not change the value of capacitance determined by the meter.

Because of the variations and unusually high values obtained for the capacitance it would be misleading to show quantitative results for the permittivity. Nevertheless, deviations relative to the initial static measurement as a function of temperature could be recorded. The qualitative curves show the relative change in dielectric permittivity which were reproducible in different samples and using different instruments. The results are displayed as a relative percent change of the permittivity at each temperature (ϵ_t) to the ambient permittivity (ϵ_a) ,or lowest value, divided by the permittivity at each temperature.

$$\% \text{ change in } \epsilon_r = (\epsilon_t - \epsilon_a)/\epsilon_t \times 10^2 \tag{44}$$

The Lock-In Amplifier (EG&G model #5101) was also used to measure the capacitance. The calculated values obtained did not agree with the negative values obtained with the electronic bridges (ignoring the sign). The values were on the order of 2.50×10^{-7} F for the polycrystalline samples to 3.75×10^{-7} F for the single crystal samples. The dielectric constants calculated from these capacitance values are listed in Table 2. These values for ϵ_r are extremely high. They are on the order of 10^3 times greater than most known ferroelectric materials.

If the instruments are reading correctly (calibrations on standard capacitors indicated they were) then the unusually large values may be real. However, the high values reflect the apparent rather than absolute values for dielectric permittivity of chalcocite. These results may be due to large inhomogeneities in the samples (Maxwell-Wagner effects) or the large number of free carriers in the material, as well as semiconducting effects inherent in chalcocite, and Schottky barrier effects at the electrode contacts. Therefore, only the qualitative behavior and relative changes in permittivity are displayed.

Alternatively, using equation (39), the series capacitance for each sample was also calculated from the inductance and resistance measurements taken with the ESI #253 Impedancemeter. The loss tangent, $\tan\delta$, for each specimen was also determined using the ESI Impedancemeter. As suspected the loss is very high for chalcocite. At 1 kHz the calculated loss angle, δ, was between 89° and 89.5° for all the samples. This implies that at 1 kHz, almost 99% of the total current is conduction current.

By assuming a loss angle of 89.25° for all the samples of chalcocite, then the parallel capacitance may be computed using equation (40). From these indirect C_p values, the dielectric constants were also calculated (Table 2). These values for ϵ_r may not be highly accurate however, their range is very realistic. These values are in the expected range for polar dielectrics. The much larger value for the single crystal specimen is to be expected, especially if oriented in the polar axis.

As was the case with conductivity in chalcocite, the dielectric permittivity shows a gradual decrease with an increase in temperature up to the region of the

Table 2. Dielectric constants of the chalcocite samples at 1 kHz. e_r - direct: calculated directly from capacitance values obtained with Lock-In Amplifier. e_r - indirect: calculated indirectly using inductance, resistance and loss factor.

Sample	e_r - direct	e_r - indirect
polycrystalline #1	5.44 x 10^5	10.8
polycrystalline #2	3.65 x 10^5	17.4
single crystal ∥ C	2.21 x 10^6	2120
single crystal ⊥ C	7.62 x 10^6	1310

transition (Figures 23, 24, 25). At the transition there is a 10% to 20% increase in permittivity.

   After the transition point the permittivity drops rapidly in an expected manner. About 40° to 50°C above the anomaly another smaller peak was also noted in most experiments. This second anomaly is suspected to be due to the tetragonal phase transition. As can be seen in Figure 25, the anomaly does have the characteristic behavior of a ferroelectric transition. It is very likely that several phases in Cu_2S are ferroelectric, and thus the behavior observed in chalcocite is similar to the situation which exists in barium titanate (Figure 29).

   Figures 23 and 24 demonstrate the reproduciblity of the dielectric behavior on consecutive experiments using the Lock-In Amplifier method. Figure 25 demonstrates how the dielectric behavior of polycrystalline sample #2 is qualitatively like that of polycrystalline #1. Therefore, the results were reproducible on separate samples. Furthermore, the method used in Figures 25

and 26 was the biasing technique with the Auto LCR Meter (ESI model #296) and Impedancemeter (ESI model #253) respectively. This demonstrates that different methods of measurement yield qualitatively reproducible results.

It was very difficult to obtain noise-free and reproducible permittivity curves for the single crystal specimen due to the high conductivity. Figure 27 shows that the dielectric behavior at 500 Hz is essentially metallic in character up to the transition point. A small peak is then followed by a large drop in permittivity; and, then a rapid, but almost linear increase in permittivity up to 200°C.

Internal pre-filters and an output voltage offset (features built into the model #5101 Lock-In Amplifier) were used to enhance the output sensitivity. Figure 28 shows the very nonlinear behavior of the permittivity up to the transition point. At both 1kHz and 10kHz a ten-fold increase in permittivity was observed. This large increase in output voltage caused a temporary saturation in the amplifier circuits of the Lock-In Amplifier; therefore, the behavior above the transition could not be recorded. After cooling, the output voltage would return to the intial value. Using the same heating rate, the transition point at 10 kHz was found to be about 10° below the transition point an 1 kHz. A shift in the Curie point towards lower temperatures is commonly observed in ferroelectrics as the frequency is increased (Lines and Glass, 1977). The results in Figure 28 may be indicative of this behavior in chalcocite.
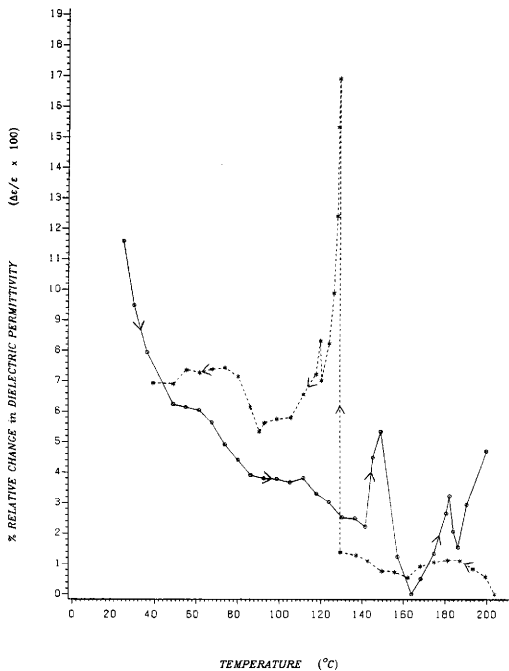
Figure 23. Dielectric behavior in polycrystalline sample #1 at 1 kHz.
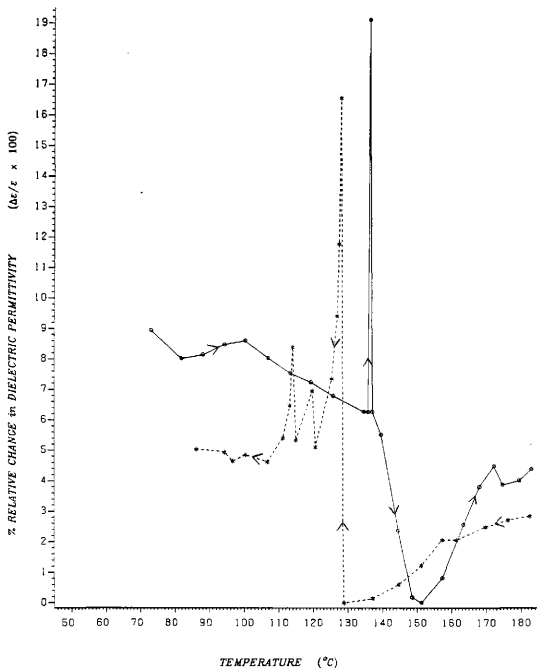
Figure 24. The dielectric anomaly in polycrystalline sample #1 at 1 kHz. Showing reproduciblity of results in Figure 23.
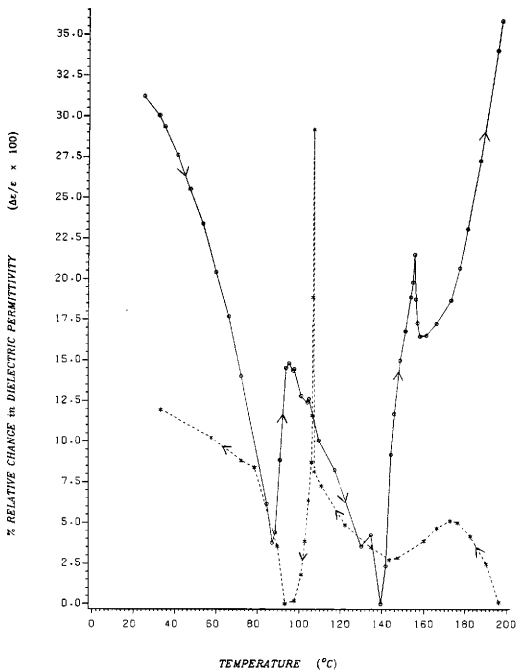
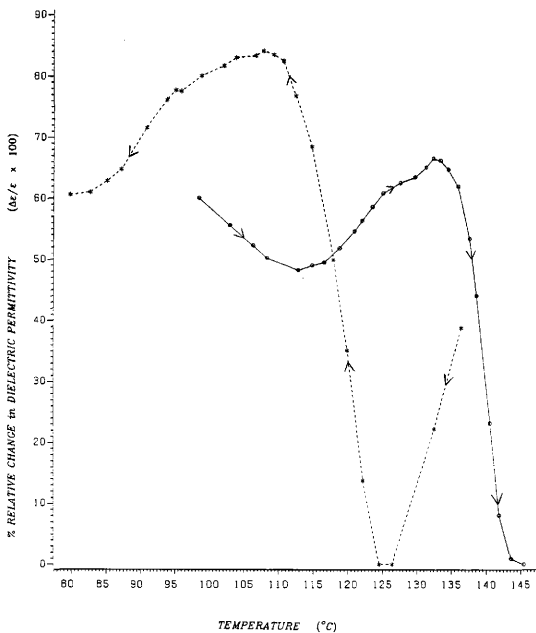Figure 25. Dielectric behavior in polycrystalline sample #2 at 1 kHz.

Figure 26. The dielectric anomaly in polycrystalline sample #2 at 1 kHz.
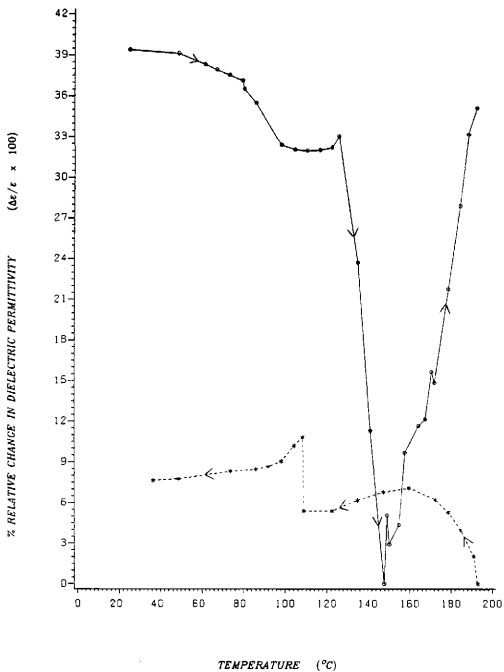
Figure 27. Dielectric behavior in single crystal ∥ to c-axis at 500 Hz.

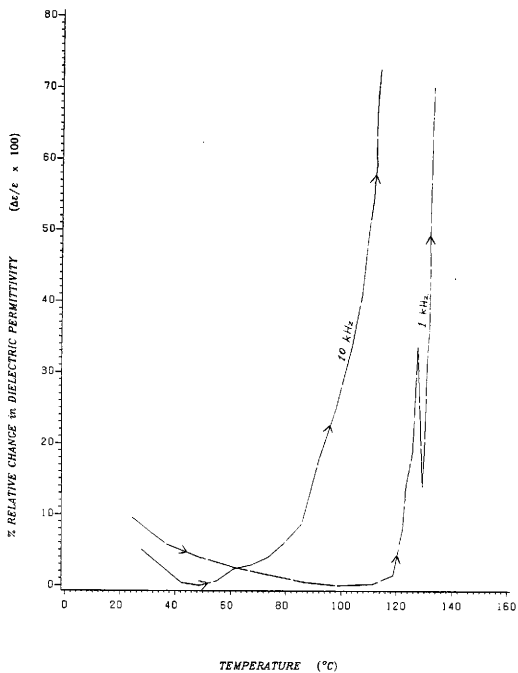Figure 28. Nonlinear dielectric behavior in single crystal ∥ to c-axis up to the transition point, at 1 kHz and 10 kHz.
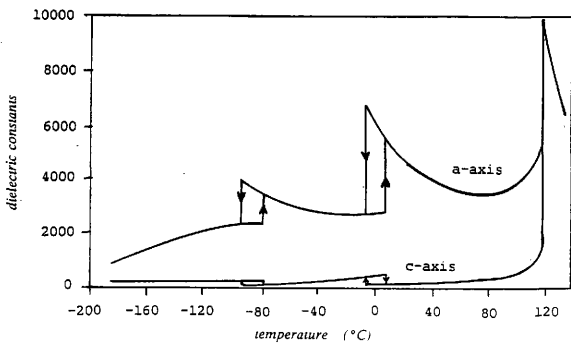
Figure 29. Dielectric constants of BaTiO$_3$ as a function of temperature (after Jona and Shirane, 1962). Shown for comparison to the anomalous dielectric behavior observed in Cu$_2$S.

Self-inductance in Chalcocite

Polycrystalline chalcocite shows metallic behavior, particularly in the region between room temperature and the phase transition. Here we see, as shown in Figures 20, 23, and 25 that both conductivity and dielectric permittivity generally decreases up to the region of the transition temperature. This is the characteristic behavior for metallic substances. In the samples used in this study, such behavior may be attributed to the presence of some amount of digenite which, as Kamigaichi (1952) describes, shows metallicity in its conductivity behavior as a function of temperature. Also, with natural specimens there are undoubtablly impurities, e.g. Fe, Ag, Fe_2O_3, etc., in the sample which will strongly effect its behavior. No quantitative analysis of the samples was undertaken.

Because of the metallic nature of the Cu_2S specimens some self-inductance is expected, and inductive effects were found. They show a temperature dependence as shown in Figure 30. The inductive behavior (Figure 30) appears to be a mirror image to the dielectric behavior shown in Figure 23. Regions of high capacitance are reflected in regions of lower inductance and vice versa.

Excessive noise was not observed but, the furnace uses a large AC field and the inductive effects tend to be amplified. The inductance effects of the furnace could be partially responsible for the differences in the curves between the heating cycles and the cooling cycles. Cooling curves were taken by shutting the power off to the furnace.
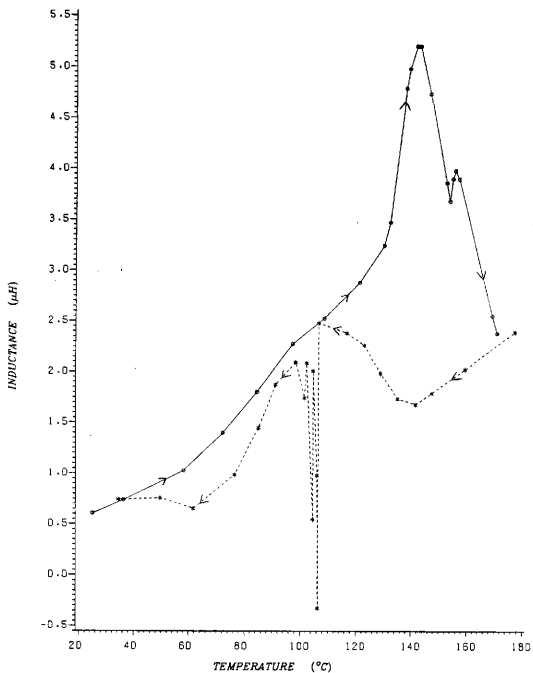
Figure 30. The inductance behavior in polycrystalline sample #2 at 1 kHz.

Dielectric Hysteresis Loop

As pointed out in chapter III, it is difficult to observe the dielectric hysteresis in materials where the conduction currents are much larger than the displacement currents. This is particularly true at low frequencies. Standard hysteresis measurements are done using 60 Hz current.

Observation of any polarization hysteresis in chalcocite proved to be difficult for these reasons. At 60 Hz the conduction current in chalcocite is essentially all the current. Therefore, a very small applied electric field quickly produces a displacement outside the range of the oscilloscope. Thus, if any hysteresis is present it could not be seen. There are alternative circuits, which may be used to compensate for conduction effects (see Lines and Glass, 1977) but this was not attempted here.

However, it was discovered that a hysteresis loop could be obtained with frequencies in the range of 10-100 kHz. Complete saturation could not be shown because of the very low resistance of the sample. The frequency generators used could not generate enough voltage to drive the current at these frequencies. Current sufficient for saturation might well damage the samples.

Figures 31 and 32 show a nearly saturated hysteresis for a single crystal specimen oriented $\perp$ to the c-axis. The temperature dependence of the hysteresis below and above the Curie point is clearly observed. The loop looses its 'S' shape and collapses above the transition. Ideally, the loop should collapse to a straight line. However, in a semiconductor the electrons and holes become displaced under an applied electric field and form dipoles. Therefore, the hysteresis effects above the Curie point may be partially due to inherent semiconducting effects and lossiness due to the high conductivity of the samples. Also, there may be some

tetragonal phase present, which if also ferroelectric, may not have completely been transformed.

Figures 33 and 34 demonstrate a directional dependence on the polarization in the same single crystal. It appears that both axes show a ferroelectric hysteresis but, the c-axis has a more pronounced effect. More than one axis may be ferroelectric, or the true polar axis is somewhere in between the two orientations sampled, or impurities and defects affect the samples.

In polycrystalline material there is an essentially random orientation of the crystal axes. If the material is ferroelectric, a hysteresis effect can be observed and, if a very strong field is applied it may be possible to reorient enough domains to observe saturation. In Figures 35 and 36 we see that polycrystalline sample #1 does display an asymmetric hysteresis which also shows a clear temperature dependence.

Although complete saturation was not obtainable with the equipment used, and may not be obtainable with so conductive a sample, the hysteresis loops obtained do qualitatively demonstrate the ferroelectric effect in the chalcocite samples tested.
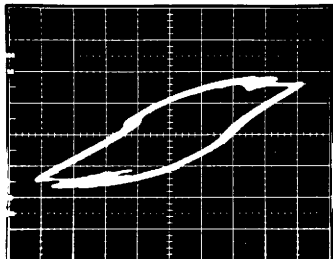
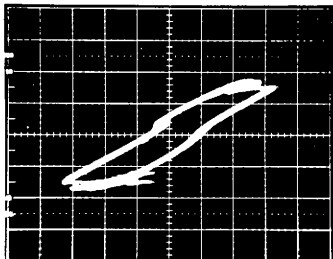Figure 31. Hysteresis loop for single crystal ⊥ to c-axis, below Curie point at 50 kHz (x = 0.2 v/div, y = 0.5 v/div).

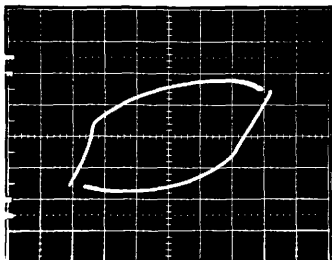Figure 32. Hysteresis loop for single crystal ⊥ to c-axis, above Curie point at 50 kHz (x = 0.2 v/div, y = 0.5 v/div).

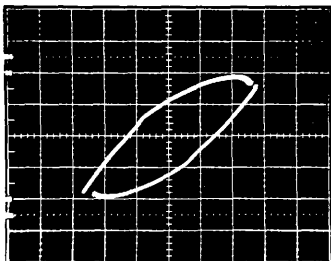Figure 33. Hysteresis loop for single crystal ∥ to c-axis at room temperature at 30 kHz (x = 0.2 v/div, y = 1.0 v/div).

Figure 34. Hysteresis loop for single crystal ⊥ to c-axis at room temperature at 30 kHz (x = 0.2 v/div, y = 1.0 v/div).
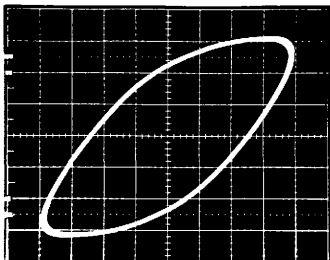
Figure 35. Hysteresis loop for polycrystalline sample #1, below Curie point at 40 kHz (x = 0.5 v/div, y = 0.5 v/div).
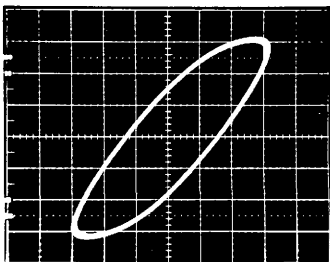

Figure 36. Hysteresis loop for polycrystalline sample #1, above Curie point at 40 kHz (x = 0.5 v/div, y = 0.5 v/div).

CHAPTER VII

CONCLUSIONS

The results of this research strongly support ferroelectricity in the samples of chalcocite tested. Qualitatively, I have shown that there is a dielectric anomaly at the order-disorder transition at 105°C. Evidence of ferroelectricity is further supported by the high frequency hysteresis loop.

It is not possible as yet to say conclusively that, in general, Cu_2S is ferroelectric. The dielectric constant must be quantitatively determined. Such determination, although attempted, was beyond the scope of this project. The reasons for failure are simple. Natural materials are full of inhomogeneities and impurities. Thus results will not be exactly consistent from sample to sample. The high conductivity of chalcocite makes it difficult to use standard techniques and equipment which were designed to measure dielectric properties of highly resistive materials.

For improved results, a better furnace with a sensitive temperature controller is required. A more carefully designed sample holder which could hold a high vacuum, withstand higher temperatures, etc., is needed. More sophisticated methods and equipment may be necessary to measure the dielectric effects in semiconductors. Ultimately, and ideally, these electrical measurements should be done on synthetically grown crystals. These should be large single crystals with no impurities and no inhomogeneities or defects.

Since there is good evidence in support of ferroelectricity in chalcocite, it would also be promising to investigate other sulfide minerals (see Corry, 1984). Ferroelectric effects may have fundamental implications for geophysical exploration for sulfides.

REFERENCES

Abdullaev, G.B., Aliyarova, Z.A., Zamanova, E.H., and Asadov, G.A., 1968, Investigation of the electrical properties of Cu_2S single crystals: Physica Status Solidi, **26**, 65-68.

Adou, J.J., and Baudet, J., 1967, Susceptibilite magnetique de composes non stoechiometriques 1.- sulfures et seleniures de cuivre et d'argent: J. Chimie Phys., **64**, 1540-1546.

Arjona, F., Elizalde, E., Feu, A., Camerero, E., Leon, M., Llabres, J., and Rueda, F., 1979, Optical and calorimetric measurements of cupreous sulphides thin films: Proc. 2nd E.C. Photovoltaic Solar Energy Conference, 903-908.

Azaroff, L.V., 1975, Introduction to solids: Robert E. Kreiger Pub. Co.

Buerger, N.W., 1941, The chalcocite problem: Econ. Geol., **36**, 19-44.

Buerger, M.J., and Buerger, N.W., 1944, Low chalcocite and high chalcocite: Amer. Mineral., **29**, 55-65.

Burfoot, J.C., 1979, Polar dielectrics and their applications: Berkeley, Univ. of Cal. Press.

Chen, T.T., and Chang, L.L.Y., 1974, Investigations in the systems Ag_2S-Cu_2S-Bi_2S_3 and Ag_2S-Cu_2S-Sb_2S_3: Can. Miner., **12**, 404-410.

Clark, S.P., 1966, Handbook of physical constants: Geol. Soc. Amer. Memoir **97**.

Cook, W.R., Jr., Shiozawa, L. and Augustine, F., 1970, The relationship of copper sulfide and cadmium sulfide phases: J. Appl. Phys, **41**, 3058-3063.

Cook, W.R., Jr., 1972, Phase changes in Cu_2S as a function of temperature: Nat. Bur. Stan. Spec. Pub. 364, Solid State Chemistry, 703-711.

Corry, C.E., 1984, Ferroelectricity in sulfides and related ore minerals: EOS, Trans. Am. Geophys. Un., **65**, 45, 1080.

Corry, C.E., 1985, Spontaneous polarization associated with porphyry sulfide mineralization: Geophys., in press.

Djurle, S., 1958, An X-ray study on the system Cu-S: Acta Chem. Scand., **12**, 1415-1426.

Duchemin, S., and Guastavino, F., 1978, Etude experimentale du seuil d'emission photoelectrique du Cu_2S massif: Solid. State Comm., **26**, 187-189.

Evans, H.T., 1971, Crystal structure of low chalcocite: Nat. Phys. Sci., **232**, 69-70.

Evans, H.T., 1979, The crystal structure of low chalcocite and djurleite: Z. Kristal., **150**, 299-320.

Evans, H.T., 1981, Copper coordination in low chalcocite and djurleite and other copper-rich sulfides: Amer. Mineral. **66**, 807-818.

Fridkin, V.M., 1980, Ferroelectric semiconductors: Consultants Bureau.

Hirahara, E., 1951a, The physical properties of cuprous sulfides-semiconductors: J. Phys. Soc. Jap., **6**, 422-427.

Hirahara, E., 1951b, The electrical conductivity and isothermal Hall effects in cuprous sulfide , semiconductor: J. Phys. Soc. Jap., **6**, 428-437.

Hurlbut, C.S. Jr., 1971, Dana's manual of mineralogy - 18th Ed.: John Wiley & Sons.

Ibragimov, N.A., Mamedov, M.Sh., and Khakimov, K., 1979, The influence of one-axis deformation on the electrophysical properties of Cu_2S at different temperatures: Dolk. Akad. Nauk Az. SSR., **35**, 23-28.

Ibragimov, N.A., Mamedov, M.Sh., and Gasanov, R.G., 1982, Effect of uniaxial deformation on electrophysical properties of $Cu_{2-x}S$ $(0 \leq x \leq 0.27)$ single crystals at different temperatures: Dolk. Akad. Nauk Az. SSR., **38**, 28-30.

Janosi, A., 1964, La structure du sulfure cuivreux quadratique: Acta Cryst., **17**, 311-312.

Jensen, E., 1947, Melting relations of chalcocite: Avhandl. Norske Videnskaps-Akad. Oslo Mat.Naturw. Klasse, **6**, 3-14.

Jona, F., and Shirane, G., 1962, Ferroelectric crystals: Macmillan.

Jost, W., and Kubaschewski, P., 1968, Spezifische warmen von silber-und kupfer(I) - chalkogeniden von - 70°C bis zu 550°C: Z. Phys. Chemie, **60**, 69-78.

Kamigaichi, T., 1952, Electrical conductivity of $Cu_{1.8}S$ (Cu_9S_5): J. Sci. Hiroshima Univ., **A16**, 325-330.

Kazinets, M.M, Ivanova, I.V., and Schafizade, R.B., 1979, Investigation of phase transformations in Cu_2S-Cu_8S thin films by kinematic electron diffraction: Phase Trans., **1**, 199-206.

Kinase, W., 1982, On the anisotropic optical properties of dielectrics and ferroelectrics: Memoirs of the Sch. of Sci. and Eng., Waseda Univ., Tokyo, no. 46, 383-396.

Kittel, C., 1976, Introduction to solid state physics: John Wiley & Sons.

Lang, S.B., 1974, Sourcebook of pyroelectricity: Gordon and Breach.

Lines, M.E., and Glass, A.M., 1977, Principles and applications of ferroelectrics and related materials: Oxford Univ. Press.

Loeb, L.L., 1961, Fundamentals of electricity and magnetism: Dover.

Luquet, H., Guastavino, F., Bougnot, J., and Vaissiere, J.C., 1972, Etude du systeme Cu-S dans le domaine $Cu_{1.78}S$-$Cu_{2.1}S$ par analyse thermique differentielle: Res. Bull., **7**, 955-962.

Marshall, R., and Mitra, S.S., 1965, Optical properties of cuprous sulfide: J. Appl. Phys., **36**, 3882-3883.

Megaw, H.D., 1957, Ferroelectricity in crystals: Methuen & Co.

Mulder, B.J., 1972, Optical Properties of crystals of cuprous sulphides: Physica Status Solidi (a), **13**, 79-88.

Mulder, B.J., 1973a, Optical properties of an unusual form of thin chalcocite (Cu_2S) crystals: Physica Status Solidi (a), **15**, 409-413.

Mulder, B.J., 1973b, Optical properties and energy band scheme of cuprous sulphides with ordered and disordered copper ions: Physica Status Solidi (a), **18**, 633-638.

Newnham, R.E., 1974, Domains in minerals: Amer. Miner., **59**, 906-918.

Nye, J.F., 1979, Physical properties of crystals: Oxford Univ. Press.

Okamoto, K., and Kawai, S., 1973, Electrical conduction and phase transition of copper sulfides: Jap. J. Appl. Phys., **12**, 1130-1138.

Olhoeft, G.R., 1981, Electrical properties of rocks, in Physical properties of rocks and minerals, II-2: Y.S. Touloukian, W.R. Judd and R.F. Roy, Ed, McGraw-Hill.

Park, C.F.Jr., and MacDiarmid, R.A., 1975, Ore deposits: W. H. Freeman.

Parkhomenko; E.I., 1967, Electrical properties of rocks; Plenum.

Parkhomenko, E.I., 1971, Electrification phenomena in rocks: Plenum.

Pickart, S.J., 1970, Physical properties of sulfide minerals: Mineral. Soc. Amer. Spec. Pap. 3, 145-153.

Picot, P., and Johan, Z., 1982, Atlas of ore mineralogy: Elsevier.

Povarennykh, A.S., 1960, On the dielectric constants of minerals: from Sci. Works Krivorog. Min. Inst., v 8.

Putnis, A., 1977, Electron diffraction study of phase transformations in copper sulfides: Amer. Mineral., **62**, 107-114.

Roseboom, E.H., Jr., 1966, An investigation on the system Cu-S and some natural copper sulfides between 25° and 700°C : Econ. Geol., **61**, 641-672.

Rothwarf, A., 1980, The CdS/Cu$_2$S solar cell: basic operation and anomalous effects: Solar Cells, **2**, 115-140.

Sato, M., and Mooney, H.M., 1960, The electrochemical mechanisms of sulfide self-potentials: Geophys., **25**, 226-249.

Sawyer, C.B., and Tower, C.H., 1930, Rochelle salt as a dielectric: Phy. Rev., **35**, 269-273.

Serebryanaya, N.R., 1966, On the tetragonal modification of chalcocite: Geochem. Internat., **3**, 687-688.

Shuey, R.T., 1975, Semiconducting ore minerals: Elsevier.

Sinkarikas, J., 1966, Mineralogy: a first course: Van Nostrand.

Skinner, B.J., 1970, Stability of the tetragonal polymorph of Cu$_2$S: Econ. Geol., **65**, 724-730.

Smykatz-Kloss, W., 1974, Differential thermal analysis; application and results in mineralogy: Springer-Verlag.

Sorokin, G.P., 1966, The chemical bond in cuprous sulphide, selenide and telluride: Russ. J. Phys. Chem., **40**, 451-453.

Starling, S.G., 1948, Electricity and magnetism: Longmans, Green and Co. Ltd.

Sumner, J.S., 1976, Induced polarization method in geophysical exploration: Elsevier.

Takeda, H., Donnay, J.D.H., Roseboom, E.H., and Appleman, D.E., 1967a, The crystallography of djurleite, Cu$_{1.97}$S: Z. Kristal., **125**, 404-413.

Takeda, H., Donnay, J.D.H., and Appleman, D.E., 1967b, Djurleite twinning: Z. Kristal., **125**, 414-422.

Ueda, R., 1949, X-ray and thermal studies on the phase transitions of cuprous sulphide Cu$_2$S: Phys. Soc. Jap., **4**, 287-292.

Vaughan, D.J., and Craig, J.R., 1978, Mineral chemistry of metal sulfides: Cambridge Univ. Press.

Wagner, G.R., Vechio, P.D., and Uphoff, J.H., 1982, Cuprous sulfide as a film insulation for superconductors: Adv. Cryog. Eng., **28**, 821-831.

Zheludev, I.S., and Sonin, A.S., 1958, Search for new ferroelectrics: Invest. Akad. Nauk S.S.S.R., Ser. Fiz., **22**, 1441-1444.

APPENDIX A

ELECTRICAL MEASUREMENTS ON SAMPLE HOLDER

The conductance and capacitance of the sample holder as a function of temperature were recorded. The electrodes were separated by approximately 1mm. Both conductance and capacitance levels were very low, showing essentially a small linear increase with temperature. Therefore, the contribution to the electrical measurements of the sample by the sample holder can be considered negligible.

Because chalcocite is very conductive, the resistance of the sample holder with the copper electrodes shorted together was also recorded. The very low resistance values shows that there was good electrical continuity in the measuring circuit. Again, essentially linear behavior was noted over the temperature range of the investigation.

Therefore, it may be concluded that any and all anomalous behavior recorded in this research can be attributed to the sample itself, although possible effects attributable to the silver electrodes, Maxwell-Wagner effects, or Schottky barriers at the metal-semiconductor contacts cannot be separated in the data.
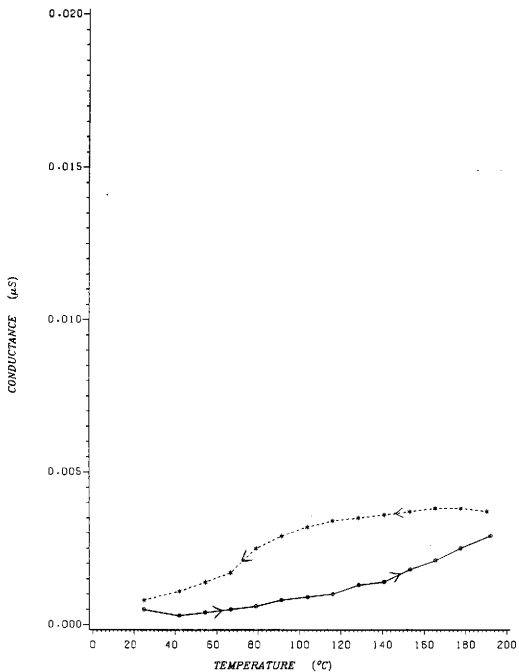
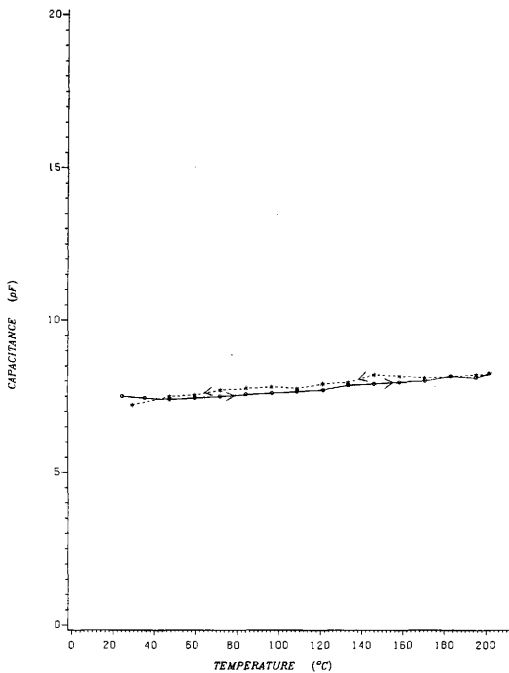Figure 37. Sample holder conductance with 1mm air gap at 1 kHz.

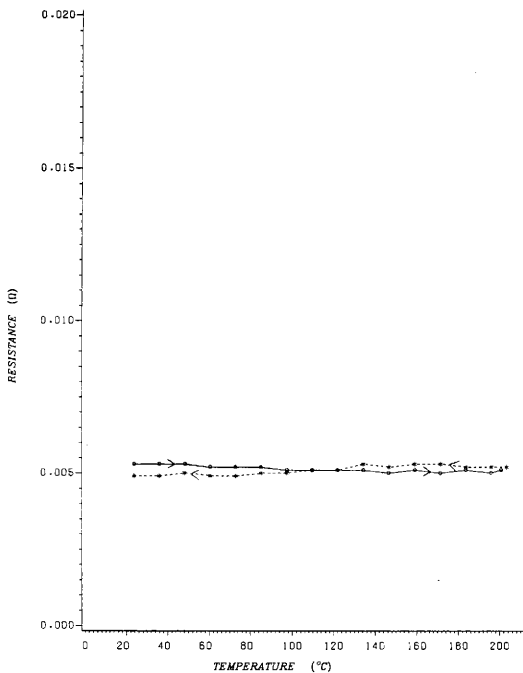Figure 38. Sample holder capacitance with 1mm air gap at 1 kHz.

Figure 39. Sample holder resistance with no air gap at 1 kHz.

APPENDIX B

INSTRUMENTATION - MODEL NUMBERS AND MANUFACTURERS

INSTRUMENT	MANUFACTURER	MODEL	DISTRIBUTOR
Impedance Bridge	General Radio	1650A	Concord, Ma.
Waveform Generator	Exact Electronics	120	Hillsboro, Or.
Impedancemeter	Electro Scientific Industries	253	Portland, Or.
X-Y Recorder	Hewlett Packard	7045B	Palo Alto, Ca.
Auto LCR Meter	Electro Scientific Industries	296	Portland, Or.
Lock-In Amplifier	EG&G Princeton Applied Research	5101	Princeton, N.J.
Oscilloscope	Tektronix	455	Portland, Or.
Chromel-Alumel Cold Junction Compensator	Omega Engineering		Stamford, Co.

VITA

The author was born in Lackawana, N.Y., October 15, 1952 to Zygmunt and Anne Bieniulis. He graduated from Frontier Central High School in Hamburg, N.Y. After which, he attended the State University College at Brockport, N.Y. and received a B.S. degree in Biology in 1974. Inspired by the natural beauty of the great southwest, he later enrolled at the University of Arizona, earning a second B.S. degree in Geosciences in 1979. After several years of working on various geophysical surveys for such companies as; Phoenix Geophysics, Zonge Engineering and Research Organization, Climax Molybdenum Co. and Goldfields Mining Corp., he enrolled in graduate school at Texas A&M University completing his work for a M.S. degree in Geophysics in 1984.

The author can be reached through his parents at the following address:

Mark Z. Bieniulis

c/o Zygmunt A. Bieniulis

S-5012 Chapman Pkwy.

Hamburg, New York 14075